Jhenifer de Farias Oliveira

BSc in Biochemistry

A 3D hepatic model to address immune-mediated drug hepatotoxicity

Dissertation to obtain the Master Degree in

Biochemistry for Health

Supervisor: Dr Catarina Brito, Principal Investigator, IBET, ITQB-NOVA

May 2021

Jhenifer de Farias Oliveira

BSc in Biochemistry

A 3D hepatic model to address immune-mediated drug hepatotoxicity

Dissertation to obtain the Master Degree in

Biochemistry for Health

Supervisor: Dr Catarina Brito, Principal Investigator, IBET, ITQB-NOVA

Jury:

President: Dr. Pedro Manuel Henriques Marques Matias

Main examiner: Dr. Ana Teresa Pinto

Examiner: Dr. Ana Maria Varela Coelho

Instituto de Tecnologia Química e Biológica António Xavier,

Universidade Nova de Lisboa

May 2021

A 3D hepatic model to address immune-mediated drug hepatotoxicity

Acknowledgments

First, I would like to acknowledge Dr Catarina Brito for letting me be part of her team and for the guidance given to me during this work. Thank you for your great leadership and for sharing your passion for science and your knowledge through this time.

I would like to specially express my gratitude to Francisca Arez who was unflagging when teaching me all the necessary methods and techniques, even the smallest details to get the best results. Thank you for sharing with me your knowledge, for all the fruitful discussions and guidance. And finally, thank you for your enthusiasm, for encouraging me and for always being available for me.

To Nuno Lopes for all the help he gave me regarding the immune cells, all the endless discussions and advice. For his availability to perform the flow cytometry analysis and for patiently teaching me how to analyze flow cytometry data and get through my results.

To Gonçalo with whom I shared a desk until we went in lockdown, so thank you for the company and for your support during this time.

To the Advanced Cell Models group, Teresa, Giacomo, Catarina, Rodrigo, Sofia, Rita, Luisa, and Isabella for making me feel welcome in the team, for showing me that I could count on them whenever I needed, for all the good advice and for the great moments of laugh.

I would like to thank all the Animal Cell Technology Unit members for the opportunity of working in this great environment where I could learn so much and feel at home.

To my master colleagues Salomé, Gonçalo, Rita, Laura, Catarina and Jéssica who have made my days lighter whenever we travelled together to/from ITQB and whenever we could have lunch together.

To my friends Leandra, Sílvia, Inês and Tatiana for always supporting me, cheering me up and believing in me. Your friendship was really important to keep me going.

To my church family, spending time with you (when it was possible) throughout this difficult year surely made it easier to get through it.

At last, but surely not at least, to the most important people in my life, my parents and my brother. You've been my biggest supporters and I wouldn't have accomplished this without you. To my parents, thank you for all the sacrifices you've done for me, for believing in me and teaching me the values I have. To my brother, thank you for the laughs and for showing me a lighter way to see life.

"*Assim, permanecem agora estes três: a fé, a esperança e o amor.*

O maior deles, porém, é o amor."

I Coríntios 13:13

Abstract

The liver is a complex organ involved in many important physiological functions. Several hepatic diseases, such as alcohol-related liver disease and drug-induced hepatotoxicity, are associated with liver inflammation. Thus, it is of extreme relevance to understand the mechanisms involved in liver inflammation to develop the best strategies to fight these diseases. The hepatic macrophages, resident Kupffer cells and monocyte-derived macrophages, are known to play a critical role in the liver inflammatory response. Although the diversity of experimental models available to address hepatic diseases has been growing, there is still a need for models that can depict the contribution of macrophages to the inflammatory response upon injury.

Having this in mind, the aim of this project was to develop a 3D cell-based model to study liver inflammatory response, by integrating the immune and hepatocyte components and assessing the effect of the heterotypic cellular crosstalk on the phenotype and functionality of both cell types. In a first step, aggregation of HepG2 cells in stirred-tank vessels, previously implemented in the lab in 125 mL-spinner vessels, was downscaled to 30 mL vessels. The HepG2 cells within the spheroids presented important features of the hepatocyte phenotype, namely the characteristic cell polarization, observed by fluorescence microscopy, and biosynthetic function, evaluated through the production of albumin. Based on the hypothesis that peripheral monocytes may differentiate into liver macrophages when in contact with hepatic cells, a co-culture of HepG2 spheroids and monocytes was established and characterized throughout 7 days of culture. Immunofluorescence microscopy showed that some monocytes infiltrated into the hepatic spheroids. Analysis of monocyte, macrophage, and KC markers by flow cytometry revealed that monocytes differentiated in co-cultures, acquiring an anti-inflammatory phenotype, as shown by the increase of the surface proteins CD163 and CD206 at day 7 of culture. These results suggest that the monocytes in contact with HepG2 cells acquired a similar phenotype as KCs after 7 days of culture.

The model here established is a first step in setting up cell models for the study of the mechanisms involved in the differentiation of monocytes recruited to the liver upon injury and their role in the development of several liver diseases.

Keywords: Liver, macrophages, Kupffer cells, inflammation, 3D culture, HepG2 cells

Resumo

O fígado é um órgão complexo envolvido em muitas funções fisiológicas importantes. Várias doenças hepáticas, como a doença hepática alcoólica e a hepatotoxicidade induzida por medicamentos, estão associadas à inflamação hepática. Como tal, é de extrema relevância compreender os mecanismos envolvidos na inflamação hepática para desenvolver as melhores estratégias de combate a essas doenças. Os macrófagos hepáticos, compostos pelas células Kupffer residentes e pelos macrófagos derivados de monócitos, desempenham um papel crítico na resposta inflamatória hepática. Embora a diversidade de modelos experimentais disponíveis para estudar doenças hepáticas tenha vindo a crescer nos últimos anos, ainda há necessidade de modelos que possam retratar a contribuição dos macrófagos hepáticos humanos para a resposta inflamatória.

Considerando o estado da arte, o objetivo deste projeto foi o desenvolvimento de um modelo celular 3D para estudar a resposta inflamatória hepática, integrando a componente imunológica e hepática, bem como a avaliação do efeito da interação celular heterotípica no fenótipo e funcionalidade dos dois tipos celulares. Num primeiro passo, a agregação de células HepG2 em frascos de agitação (*spinners*), previamente implementado no laboratório em frascos de 125 mL, foi reduzida para frascos de 30 mL. As células HepG2 nos esferóides apresentaram características importantes do fenótipo hepático, nomeadamente a polarização celular, observada por microscopia de fluorescência, e função biossintética, avaliada através da produção de albumina. Com a hipótese de que monócitos periféricos em contato com células hepáticas se diferenciam em macrófagos hepáticos, estabeleceu-se uma co-cultura de esferoides de HepG2 e monócitos, que foi caracterizada ao longo de 7 dias. As imagens de microscopia de imunofluorescência mostraram que alguns monócitos infiltraram os esferoides hepáticos. A análise de marcadores de monócitos, macrófagos e KC por citometria de fluxo revelou que em co-cultura, os monócitos se diferenciaram. O aumento das proteínas CD163 e CD206 na superfície celular do dia 0 para o 7º dia de cultura sugere que os monócitos adquiriram um fenótipo anti-inflamatório. Estes resultados sugerem que os monócitos em contato com células HepG2 adquiriram um fenótipo semelhante ao das KCs.

O modelo aqui estabelecido é um primeiro passo na criação de modelos celulares para o estudo dos mecanismos envolvidos na diferenciação de monócitos recrutados para o fígado após lesões e seu papel no desenvolvimento de diversas doenças hepáticas.

Palavras-chave: Fígado, macrófagos, células Kupffer, inflamação, cultura 3D, células HepG2

Contents

Figure Index

Table Index

Abbreviations

AAG	a-1-acid glycoprotein
AhR	Aryl hydrocarbon receptor
Arnt	Aryl hydrocarbon receptor nuclear translocator
AFU	Arbitrary Fluorescence Units
ALD	Alcoholic liver disease
APAP	Acetaminophen
BLCs	Biliary-like cells
CCL	C-C chemokine ligands
CCR	C-C chemokine receptors
CD	Cluster of differentiation
CLD	Chronic liver disease
Con-A	Concanavalin A
CRP	C reactive protein
CYP	Cytochrome P450
2D	Two-dimensional
3D	Three-dimensional
DAMPs	Damage-associated molecular patterns
DAPI	4′,6-diamidino-2-phenylindole
DCs	Dendritic cells
DILI	Drug induced liver injury
DMEM	Dulbecco's Modified Eagle's Medium
DNA	Deoxyribonucleic acid
ECM	Extracellular matrix
EDTA	Ethylenediamine tetraacetic acid
FBS	Fetal bovine serum
FDA	Fluorescein diacetate
FITC	Fluorescein isothiocyanate
FSC-A	Forward Scatter Area
FSC-H	Forward Scatter Height
FSG	Fish Skin Gelatin
$GdCl_3$	Gadolinium chloride

HLCs Hepatocyte-like cells

HNF4α Hepatocyte nuclear factor 4 alfa

HSCs Hepatic stellate cells

iDILI Idiosyncratic DILI

ID3 Inhibitor of DNA

IFN-γ Interferon gamma

IgG Immunoglobulin G

IL Interleukin

iNOS Inducible nitric oxide synthase

iPSCs Induced Pluripotent stem cells

KCs Kupffer cells

KLCs Kupffer-like cells

LPS Lipopolysaccharide

LSECs Liver sinusoidal endothelial cells

LXR-α Liver X receptor-α

Mφs Macrophages

MARCO Macrophage Receptor with Collagenous structure

MCP-1 Monocyte chemoattractant protein-1

MFI Median fluorescence intensity

MIP Macrophage Inflammatory Protein

miR microRNA

MPCC Micropatterned co-culture

MRP2 Multidrug-resistance-associated protein 2

MSCs Mesenchymal stem cells

NASH Nonalcoholic steatohepatitis

NK Natural Killer cells

NKT Natural Killer T cells

NO Nitric oxide

NPCs Non-parenchymal cells

PAMPs Pathogen-associated molecular patterns

PBMCs Peripheral blood mononuclear cells

PBS Phosphate-buffered saline

Pen/Strep Penicillin – streptomycin

PFA Paraformaldehyde

PHH Primary human hepatocytes

PI Propidium iodide

RI Replacement index

ROS Reactive oxygen species

SAA2 Serum amyloid A2 protein

SCID Severe combined immunodeficiency

SSC-A Side Scatter Area

TGF Transforming growth factor

TLR4 Toll-like receptor 4

TNF Tumor necrosis factor

TX-100 Triton X-100

ULA Ultra-low attachment

uPA urokinase-type plasminogen

VCAM-1 Vascular Cell Adhesion Molecule-1

VSIG4 V-set and Immunoglobulin Domain Containing 4

1. Introduction

1.1. Liver: components and functions

The liver is a vital organ with major physiological functions, such as the metabolism of carbohydrates, lipids and proteins and the detoxification of the blood[1,2]. Moreover, the liver plays an important role in the metabolism of xenobiotics, since hepatocytes express many of the enzymes and transporters involved in this process[3–6], as described below.

The liver is composed of hepatocytes, which are the parenchymal cells and constitute 60-80 % of the cells in the human liver, and of non-parenchymal cells (NPCs)[7]. The population of NPCs is comprised of: liver sinusoidal endothelial cells (LSECs, approximately 50 %); Kupffer cells (KCs, 20 %), the resident macrophages (Mφs); hepatic stellate cells (HSCs, 1%); liver dendritic cells (DCs, 1%); cholangiocytes (5%), the biliary cells; and intrahepatic lymphocytes (25%), such as the natural killer cells (NK), the natural killer T cells (NKT) and the γδ T cells[7–9]. The interaction of the parenchymal and non-parenchymal compartments is crucial for the function of the liver, as NPCs are reported to improve the maintenance of hepatocytes' differentiated phenotype[10–12]. Moreover, as reviewed in Godoy *et al*, NPCs positively influence hepatocyte functions, e.g., by inducing cytochrome P450 (CYP450) expression or the acute phase response of hepatocytes[13].

1.1.1. Hepatocytes

Hepatocytes, the effector cells of the liver, are polygonal-shaped cells[14] that are aligned between a capillary network as cords around the central vein, creating a hexagonal-shaped lobule[15]. At each vertex of the lobule, there is a portal triad, which consists of branches of the portal vein, bile duct, and hepatic artery (Figure 1.1)[15].

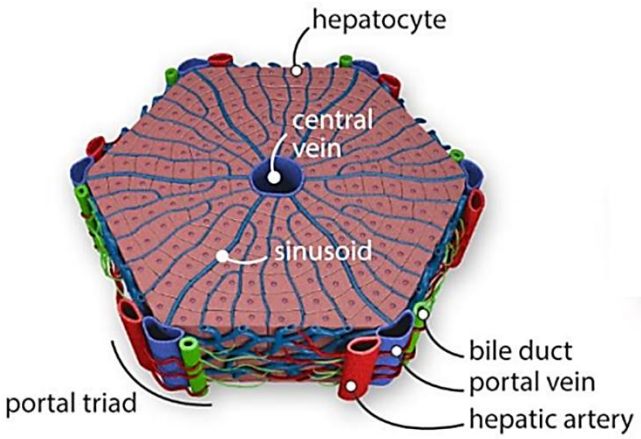

Figure 1.1. Illustration of the structure of a liver lobule. The liver lobule has a central vein from which the sinusoids and hepatocytes radiate, creating a hexagonal shape. The vertices of the hexagon have portal triads formed by a bile duct, a portal vein and a hepatic artery. Adapted from Grunsven (2017).

The lobule is the basic functional unit of the liver and is characterized by a functional zonation[15]. This consists of differentially functionalized hepatocytes according to the proximity to the central vein or the hepatic artery, as shown in figure 1.2[16,17].

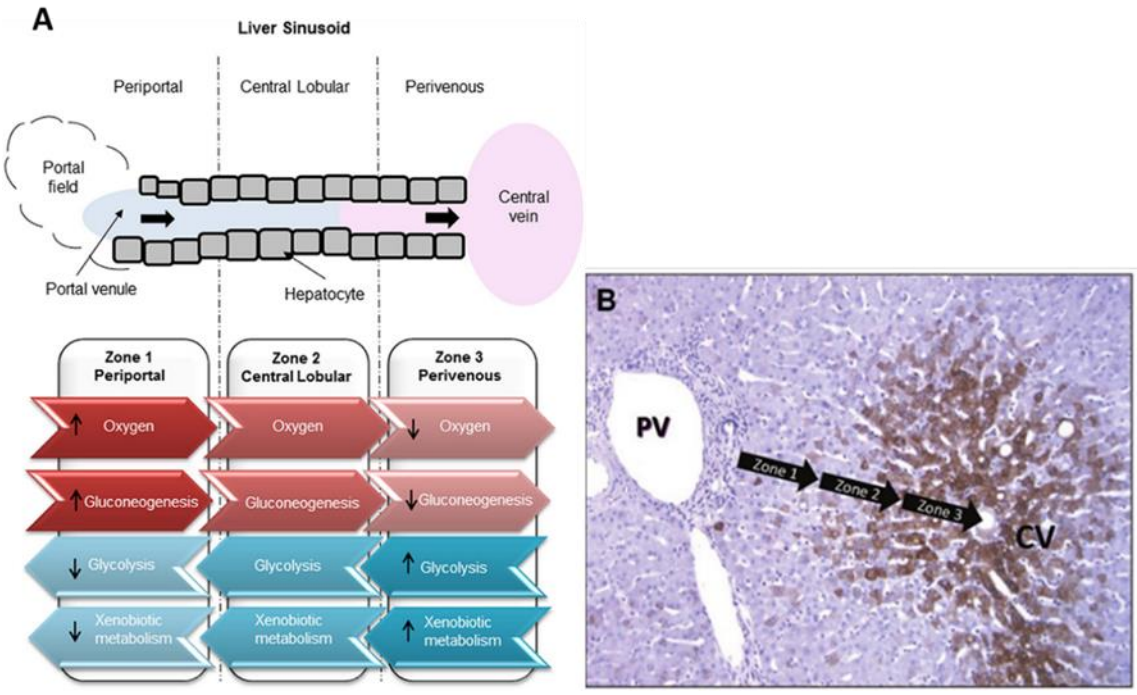

Figure 1.2. Liver zonation (A) Schematic of the liver zonation and corresponding functionalities; **(B)** Immunostaining of human liver tissue with an antibody against CYP3A4 (brown), showing the differential expression of CYP enzymes across the zones of the liver microstructure. Adapted from Tomlinson *et al.* (2019), Frontiers in Bioengineering and. Biotechnology and Lecluyse *et al.* (2012), Critical Reviews in Toxicology.

Functions such as gluconeogenesis and urea production are associated with the periportal section, while xenobiotic metabolism, glycolysis and glutamine synthesis are linked to the perivenous portion of the liver[18]. Regarding xenobiotic metabolism, hepatocytes express drug-metabolizing enzymes, which are classified into two main groups, phase I and phase II[19,20]. The enzymes from phase I include mostly CYP450 enzymes and flavin-containing monooxygenase isoforms. These increase the polarity of drugs by adding or exposing a polar group, normally through oxidation, reduction, or hydrolysis reactions[19,20]. Phase II metabolizing enzymes (e.g., glutathione S-transferase, glucuronosyltransferase, N-acetyltransferase, etc.) enhance the polarity of the drugs or their metabolites after phase I reactions, by conjugation with molecules such as glutathione[19,20]. This process leads to the biotransformation of the parent compound, to increase their lipophilicity and consequently excretion by drug transporters, which is considered the phase III (e.g., Multidrug-resistance-associated protein 2, MRP2)[21]. Another of the major functions of the liver is the production of serum proteins, of which albumin is the most abundant one. Albumin is responsible for the maintenance of the oncotic pressure of the blood and the transport of several molecules in the plasma, including drugs[22–24]. Experimentally, the secretion of this protein is often a readout of hepatocyte biosynthetic function[25]. Another marker often used for the characterization of hepatocytes is the hepatocyte nuclear factor 4 alfa (HNF4α), a transcription factor with an important

role in the hepatic identity. HNF4α regulates the expression of multiple hepatic genes, such as albumin and those involved in glucose, fatty acid, cholesterol, and drug metabolism[26,27], being essential for the functional differentiation of hepatocytes[28,29]. Furthermore, HNF4α triggers the formation of tight junctions during liver development[30], which are important for hepatocyte polarity. Hepatocytes are distinguished for being highly polarized cells, characterized by lateral, basal, and apical domains spatially segregated by tight junctions (Figure 1.3).

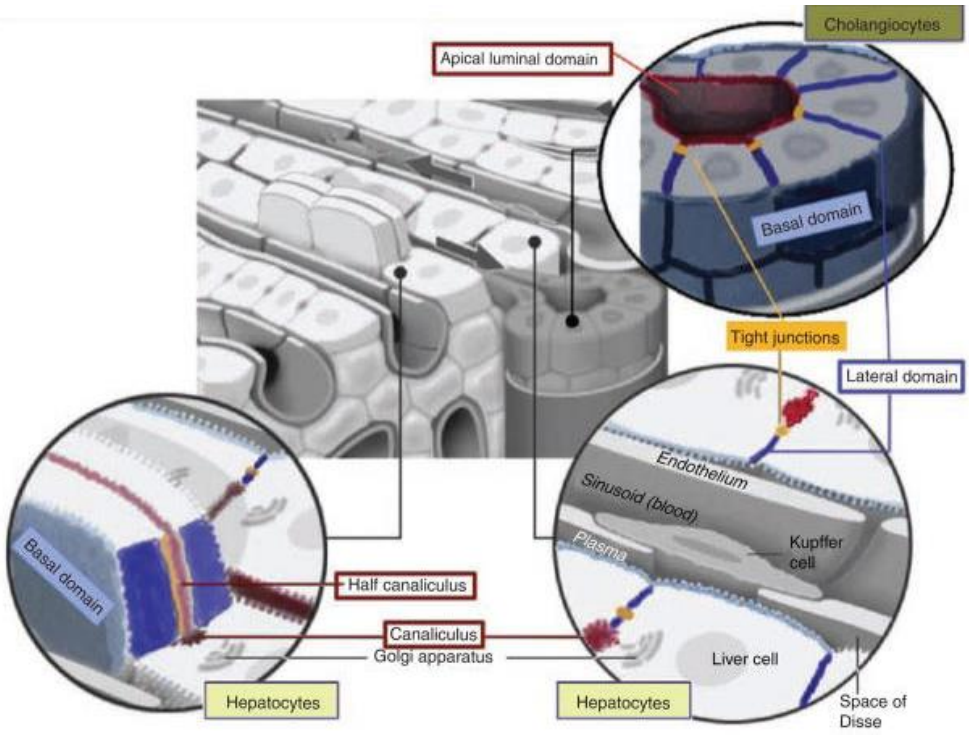

Figure 1.3. Schematic of the domain organization of hepatocytes. Red: luminal domains, dark blue: lateral domains engaged in cell-cell adhesion, gray: basal domain, facing the space of Disse, yellow: tight junctions. Adapted from Treyer *et al.* (2013).

The lateral domain is responsible for cell-cell contacts, while the basal domain mediates the cell-extracellular matrix interactions (ECM). These are often referred to as the basolateral membrane. Additionally, along the lateral cell-cell contacts, in the apical domain, hepatocytes form narrow lumens between adjacent cells termed bile-canaliculi, which are delimited by tight junctions[31]. Specific transporters that excrete drugs and the bile secreted by hepatocytes are localized in these tight junctions[31]. One of the ways to experimentally detect these canalicular structures and thus, evaluate hepatocyte morphology *in vitro* is through the detection of MRP2, which localizes at the apical membrane[32]. A simpler approach is the detection of F-actin rich regions at the cellular junctional sites delineating these bile canalicular structures[18].

1.1.2. Innate immune cells in the liver

The liver innate system is composed of KCs, the resident Mφs, DCs, NKs and NKT cells[33]. Together with the antimicrobial effector molecules (inflammatory cytokines, chemokines, acute phase proteins, complement) they coordinate to eliminate invading pathogens and damaged host cells[33].

KCs are the predominant Mφs in the liver and its first line of defense, since some of the KCs reside in the periportal region, where there is transport of systemic bacteria and bacterial products from the gut to the liver[33]. Thus, the resident Mφs are mainly responsible for clearing circulating endotoxins, microorganisms, viruses, dead cells and debris through phagocytosis[34–39]. It has been reported that KCs originate from erythromyeloid progenitors that during embryogenesis are generated in the yolk sac and migrate to the nascent fetal liver[40]. The body of research on the characterization of the liver-resident macrophage populations relied on mice models. Recently, MacParland *et al*. reported the first study on the human liver. The authors resourced to single-cell RNA-sequencing to profile the cell populations of the human liver, shedding new light on the distinct intrahepatic macrophage populations[41]. The Mφs (defined as cluster of differentiation (*CD)68*-expressing cells) were categorized into two distinct populations: immunoregulatory KCs, which presented increased expression of genes from pathways related with immune tolerance, such as the V-set and immunoglobulin domain containing 4 gene (*VSIG4*) and *CD163,* and that were defined by the expression of the macrophage receptor with collagenous structure gene (*MARCO*), amongst other genes; proinflammatory Mφs, that revealed a transcriptional profile similar to that of recently recruited macrophages[41] (e.g., decreased expression of *CD163* and increased expression of genes involved in inflammatory pathways), as previously reported in mice[42]. To examine functional differences between both Mφ populations, tumor necrosis factor (TNF)-α secretion was assessed via intracellular cytokine staining after each population was stimulated *in vitro* with lipopolysaccharide (LPS) and interferon (IFN)-γ. The results demonstrated that $MARCO^+$ Mφs secreted less TNF-α in response to stimulation than $MARCO^-CD68^+$ Mφs, suggesting that the latter are more pro-inflammatory, thus consolidating the previous observations in gene profile[41]. MARCO is a class A scavenger receptor involved in phagocytic cell-mediated innate immune responses[43,44]. VSIG4 is a complement receptor and has been shown to act as a co-inhibitory ligand that induces tolerance in liver T-cells and NKT-cells in mice upon liver injury[45]. MARCO and VSIG4 were selected as KCs-specific markers to perform the characterization of the immune cells in this thesis work, along with monocyte markers (CD14, CD16), markers for M1-phenotype (CD80) and M2-phenotype (CD163, CD206).

Human liver DC originate from bone marrow precursors[46] and are responsible, together with KCs, for initiating the innate immune response against invading pathogens or liver injury[33]. KCs and DCs possess pattern recognition receptors that recognize pathogen-associated molecular patterns (PAMPs), including components of invading pathogens, such as LPS or damage-associated molecular pattern molecules (DAMPs), such as endogenous ligands released by damaged host cells[33]. Upon activation,

KCs mostly act through the production of reactive oxygen species (ROS) and by releasing proinflammatory cytokines such as interleukin (IL)-1β, IL-6, TNF-α and transforming growth factor (TGF)-β, which will further activate and recruit other immune cells, such as neutrophils and monocytes[46].

Monocytes and neutrophils, which originate from a common myeloid progenitor in the bone marrow, circulate in the blood stream as non-differentiated cells and are the first circulating immune cells to arrive to the foci of the injured liver[33]. Following recruitment, monocytes can differentiate into Mφs or myeloid DCs which may replenish the existing populations, contributing to homeostasis, host defense, tissue remodeling, and repair[33].

1.1.3. Liver macrophages: Kupffer cells and macrophages derived from circulating monocytes

In humans, there are three populations of blood circulating monocytes identified by the expression of the surface markers CD14 and CD16: $CD14^{++}$(high detection), $CD16^{-}$(negative) for classical; $CD14^{++}$, $CD16^{+}$(positive) for intermediate; $CD14^{+}$, $CD16^{++}$ for non-classical[48–50]. The differential expression of these surface receptors corresponds to either a proinflammatory (non-classical) or anti-inflammatory (classical) phenotype[51].

Several studies have demonstrated that upon liver injury monocytes are recruited to the damaged tissues, and differentiate into diverse myeloid cells, such as monocyte-derived Mφs[52–54]. A study comprising 226 patients with chronic liver disease (CLD), showed an increase of blood circulating monocytes, in particular $CD14^{+}CD16^{+}$ inflammatory/non-classical monocytes, compared to healthy controls (184 donors). Increased circulating monocyte counts correlated with disease progression, and there was a significant accumulation of infiltrating $CD14^{+}CD16^{+}$ cells in the cirrhotic liver[52]. This monocyte subset was correlated with the release of proinflammatory cytokines, such as TNF-α and C-C chemokine ligand 4 (CCL4), also known as macrophage inflammatory protein (MIP) 1-β, revealing its contribution to the perpetuation of intrahepatic inflammation[52]. Moreover, C-C chemokine receptors (CCR) 1, 2 and 5, the receptors for CCL3/MIP1α, CCL2 (or monocyte chemoattractant protein-1 – MCP-1) and CCL4 (or MIP1β), respectively, were upregulated in the fibrotic livers[52]. The mRNA of *ccl2* and *ccl5* was upregulated in the fibrotic liver and the serum concentrations of CCL3 and CCL4 were increased in CLD patients[52]. Therefore, the authors suggested that the recruitment and differentiation of those monocytes were regulated by chemokine signaling. CCL2, for instance, has long been identified as a chemoattractant for monocytes[55], being responsible for the activation of several intracellular signaling cascades related to cell migration, such as the JAK2/STAT3[56,57] and MAPK[58] signaling pathways. Miura *et al.* found that the mRNA of *ccl2* and its receptor, CCR2, were upregulated in infiltrated Mφs isolated from livers of mice with nonalcoholic steatohepatitis (NASH)[59]. Furthermore, $CCR2^{-/-}$ mice showed reduced hepatic Mφ infiltration, highlighting the relevance of this receptor in monocyte recruitment[59]. Heymann *et al.* revealed another chemokine receptor involved in this process,

CCR8, which was upregulated upon injury in liver macrophages. These exhibited higher migratory activity compared with macrophages from CCR8$^{-/-}$ mice[60]. Besides liver injury caused by chronic or acute diseases, liver infection is another situation that triggers monocyte recruitment into the liver. A well-described example of this scenario is the infection by *Listeria monocytogenes* (reviewed in Serbina *et al.*, 2012[61]). Blériot *et al.* (2015) showed that KCs, which capture the bacteria, undergo necroptosis leading to the depletion of the resident Mφ pool and recruitment of circulating monocytes. The latter, in a first step, differentiated into M1-Mφs to control the bacterial load and then shifted to an M2 phenotype, differentiated into new KCs, replenishing the liver as resident Mφs[62]. In this study, the authors proposed IL-33 as the cytokine involved in this recruitment. Their results demonstrated that KCs necroptosis triggers hepatocytes to release IL-33, which in turn triggers IL-4 production by basophils, leading to the proliferation and M2 differentiation of recruited monocyte-derived macrophages[62].

The mechanisms and factors associated with monocyte differentiation into KCs in the liver are unknown. As such, the interest in this matter has been growing and researchers have been trying to characterize this phenomenon, mostly employing mice models. A study from Scott *et al.* suggested that bone marrow-derived monocytes can give rise to self-renewing KCs if the niche is available. Using a mice model of diphtheria toxin-mediated depletion of KCs[42], the authors showed that these monocyte-derived KCs presented matching phenotypical and transcriptional features with embryonic KCs. The features included similar size and granularity, equal phagocytic capacity and expression of the 100 most enriched genes in embryonic-KCs[42]. The authors also observed monocyte-derived KCs in livers of postnatal mice, suggesting that besides the cells from embryonic origin, monocyte-derived KCs may also contribute to the niche of KCs found in adult mice[42]. Another study by the same group demonstrated that the combined actions of HSCs and LSECs are essential for the monocyte infiltration and differentiation into KC-like cells[63]. Their results showed that upon KCs loss, HSCs and LSECs are activated by TNFα and IL-1, which in turn produce chemokines and adhesion molecules, such as CCL2, and Vascular Cell Adhesion Molecule-1 (VCAM-1), responsible for the monocyte engraftment[63]. Furthermore, HSCs and LSECs along with hepatocytes induced the expression of the transcription factors inhibitor of DNA binding 3 (ID3) and liver X receptor-α (LXR-α), which were shown to control the identity of KCs[64,65]. Figure 1.4 sums up the achievements of this study.

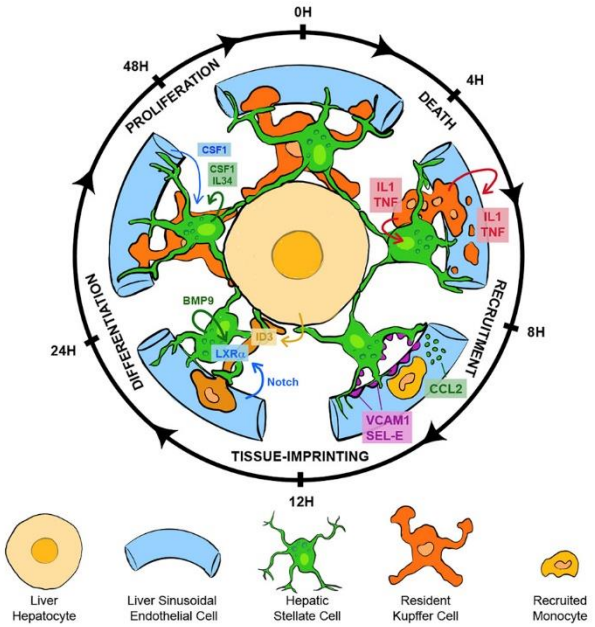

Figure 1.4. Mechanisms involving monocyte recruitment, differentiation, and proliferation in the liver upon Kupffer cell loss. Injured KCs release IL-1 and TNF, activating LSECs and HSCs, which in turn secrete CCL2, VCAM-1 and SEL-E. The latter are responsible for the recruitment of monocytes to the site of injury, which will acquire the KC identity through the action of LXRα, ID3 and BMP9, secreted by LSECs, hepatocytes and HSCs, respectively. After differentiation, monocyte-derived KCs proliferate through the combined actions of CSF1 and IL34, secreted by LSECs and HSCs. KCs (Kupffer Cells), IL-1 (Interleukin-1), TNF (Tumor Necrosis Factor), LSECs (Liver Sinusoidal Endothelial Cells), HSC (Hepatic Stellate Cells), CCL2 (C-C motif chemokine ligand-2), VCAM-1 (Vascular Cell Adhesion Molecule-1), SEL-E (Selectin-E), BMP9 (Bone Morphogenetic Protein 9), CSF1 (Colony Stimulating Factor-1), IL34 (Interleukin-34), LXRα (Liver X receptor-α), ID3 (Inhibitor of DNA binding 3). Graphical abstract from Bonnardel *et al.*, 2019.

1.1.4. Kupffer cells in liver diseases and drug metabolism

Although essential for the maintenance of the liver physiological microenvironment, the activation of KCs is associated with liver injury. In fact, many liver pathologies, such as drug-induced liver injury (DILI) and alcoholic liver disease (ALD), are reported to be mediated by the interaction of parenchymal cells with non-parenchymal cells, such as KCs and HSCs[66–68].

Adachi *et al.* showed that KC inactivation prevents the pathological effects of ethanol in the organ, such as steatosis, inflammation and necrosis[69]. The authors suggested that KCs may have a role in the development of ALD by stimulating ethanol metabolism in hepatocytes, which requires oxygen, consequently causing pericentral hypoxia[69].

In another study, Sass *et al.* treated mice with concanavalin A (Con-A), which causes severe TNF-α–and IFN-γ–mediated liver injury, to study the role of nitric oxide (NO) in liver damage[70]. TNF-α and IFN-γ are known to induce inducible nitric oxide synthase (iNOS). The study showed that the expression of the iNOS gene was upregulated in both hepatocytes and KCs after Con-A treatment[70], demonstrating that both cell types were activated through the pathways. The authors also demonstrated that the TNF-α- and IFN-γ-mediated activation of KCs upon liver injury contributed to the progression of the inflammation.

Besides their role in liver disease, KCs also play an important role in drug metabolism. A clear example was reported by Ding *et al*. in mice with hampered KC functionality through gadolinium chloride (GdCl3) injection[71]. The total CYP450 content and the activities of CYP2E1 and CYP3A were assessed 1 day after injection, showing already some reduction, after 3 and 6 days[71]. In the same study, this inhibitory effect was reverted by treatment with an immunomodulatory polysaccharide derived from the root of *Angelica sinensis*, which activated KCs, leading to restored metabolic activity[71]. Another study has shown the influence of KCs on specific CYP450 isoforms, such as CYP1A2. LPS-treated co-cultures of rat hepatocytes and KCs showed a downregulation at gene and protein levels of the CYP1A2 and of transcriptional activators of CYPs, namely the nuclear receptor aryl hydrocarbon receptor (AhR) and the AhR nuclear translocator (Arnt), which was not observed in hepatocyte monocultures[72]. This downregulation was attenuated by anti-TNFα and anti-IL-1β blocking antibodies, suggesting that proinflammatory cytokines released by KCs were involved in the downregulation of CYP1A2[72].

DILI is a hepatotoxic injury induced by the toxicity of drugs or their metabolites. The symptoms of this disease include weakness, poor appetite, dark urine and fever[73]. This disease is one of the major causes of the withdrawal of drugs from the market[74–77]. Acetaminophen (APAP), or paracetamol, is one of the most widely used drugs to experimentally demonstrate DILI. Wang *et al.* demonstrated that hepatocyte necrosis caused by APAP toxicity releases DAMPs, which can interact with toll-like receptor 4 (TLR4) to induce inflammation[78]. It has been shown that KCs are activated by DAMP molecules, possibly via TLR signaling, inducing ROS production and secretion of other inflammatory mediators. This process leads to the recruitment of other immune cells to the site of injury, perpetuating the damage observed in DILI (Figure 1.5)[79].

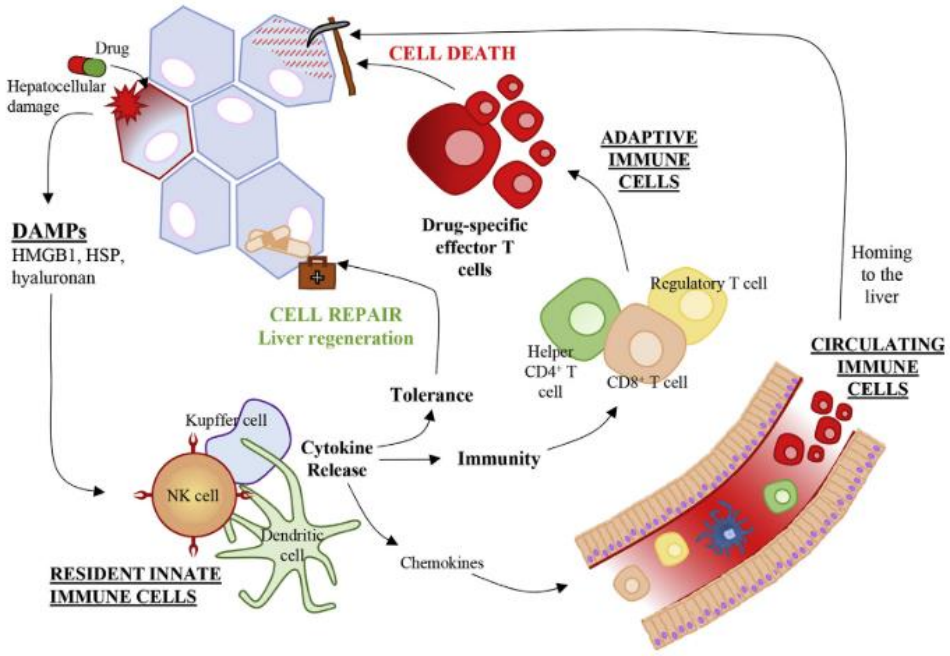

Figure 1.5. Representative scheme of immune-mediated drug-induced liver injury (DILI). The hepatocyte damage caused by a drug triggers the release of DAMPs, activating the innate immune cells**.** These activated cells can either work towards cell repair by the production of IL-10, IL-13, and TGFβ or contribute to inflammation by

secreting TNFα, IL-β, and IFN-γ. The adaptive immune cells, that can be recruited from circulation, can perpetuate the hepatic injury. DAMPS **(**Damage-associated Molecular Patterns), IL-10 (Interleukin-10), IL-13 (Interleukin-13), TGFβ (Transforming Growth Factor-β) TNFα (Tumor Necrosis Factor-α), IL-β ((Interleukin-β), IFN-γ (Interferon-γ). Adapted from Waddington *et al.* (2018).

The broad involvement of KCs in the liver response to drugs, as well as in the disease progression, highlights the importance of accounting for these cells in experimental models of disease as well as models for drug development, to more accurately predict immune-mediated DILI.

1.2. Experimental Models

In this section, some of the models designed to recapitulate the liver or some of its functions, will be presented, as well as their usefulness/application in the study of liver diseases and/or in drug testing. These models can be divided into *in vivo* (animal models) and *in vitro* (cell culture models), the latter can be two- or three-dimensional (2D and 3D, respectively) cultures.

1.2.1. Animal models

Studies on the pathophysiological mechanisms of liver diseases and drug metabolism have been employing animal models. Among the available animal models, mice and rats are the most commonly used, since the entire genome of the mouse is known and 99% similar to the human genome[80]; rodents have a short reproductive cycle and a lower maintenance cost; they can carry different mutations, and their small size makes them easy to handle[81,82]. Animal models can address systemic effects or responses, with the integration of the immune and endocrine systems, which release soluble factors that can affect the liver response to a drug or injury[83]. However, animal models present significant differences in drug pharmacokinetics and pharmacodynamics in comparison to humans[1]. Olson *et al*, studied toxicity to 150 compounds and showed that rodents are predictive of 43 % of human toxicity, while nonrodents (dogs and primates) are predictive of 63%[84].

To overcome interspecies variability, chimeric humanized mice are alternative models. Human cells are injected in immune-deficient mice to repopulate the organ of interest [85]. Regarding liver models, a study by Guo *et al.* demonstrated a successful human hepatocyte repopulation of the mouse liver upon transplantation. The authors reported that the human hepatocytes in the mouse produced human albumin, expressed alpha-fetoprotein transcripts and metabolic enzymes, such as CYP1A2 and UGT1A1[86]. Tateno *et al.* used transgenic urokinase-type plasminogen activator severe combined immunodeficiency (uPA/SCID) mice in their study, which are characterized by a severe hypofibrinogenemic state and accelerated hepatocyte death triggered by urokinase over-production in the liver[87]. They demonstrated liver repopulation of uPA/SCID mice transplanted with human hepatocytes, achieving a replacement index (RI) as high as 96%. However, the mice had to be treated with a drug that has anti-human

complement factor activity to survive with RI >50%. The transplanted hepatocytes expressed mRNAs of human CYPs, among other human genes. Specifically, CYP3A4 and CYP1A1/2 were up-regulated when the mice were treated with known inducers, rifampicin and 3-methylcholanthrene, respectively[88]. However, humanized models present some drawbacks: for instance, they can present low levels of B cells or impaired immune responses to antigens[89], which compromises addressing the impact of immune responses in drug metabolism. Also, the host innate immunity often impairs engraftment. Furthermore, humanized mice models are produced at high costs due to the costly stem cells, primary human hepatocytes used for grafting and the specific conditions they may require[90].

Despite the promising results achieved with animal models, especially chimeric mice, overall, the lack of accuracy representing human immune responses[91] in the current animal models is still a drawback that must be overcome. Taking into consideration the disadvantages of animal models discussed above, in addition to the ethical issues, there is a constant search for alternative models.

1.2.2. *In vitro* human models

Many cell sources can constitute *in vitro* models, such as primary human cells, immortalized hepatoma cell lines, stem cell-derived (adult or embryonic) and human induced pluripotent stem cells (hiPSC). Beyond that, these models can be based on different culture systems that go from simple well plates to complex bioreactors.

1.2.2.1. Cell sources

Primary human hepatocytes (PHH) are obtained from liver biopsies, surgical resection and marginal livers, and they have been reported to retain *in vivo* drug biotransformation activity. The use of PHH to study the liver overcomes the issue of interspecies differences observed in animal models. Therefore, PHH have been the gold standard *in vitro* model for toxicological studies[92,93]. The major disadvantages of this cell source are the reduced availability associated with primary material and the high costs of commercially available cells. The inter-donor variability can be both a disadvantage, in a way that is harder to systematize an efficient treatment, and an advantage since it enables the identification of potential toxic effects that will only occur in a portion of the patients. Another disadvantage of PHH is their dedifferentiation, which can be reverted with complex culture systems[94–96]. The latter will be addressed in section 1.2.2.2.

Human hepatoma cell lines, which reconstitute some of the functions of differentiated hepatocytes, have been used as an alternative for PHH. These cell sources have a long lifespan, are highly available, easy to handle, scalable and cheaper than PHH[97–99]. Among the several available hepatoma cell lines, HepG2 and HepaRG cells are the most widely used[100,101]. A study by Berger *et al.* compared the metabolic activity of PHH, HepaRG and HepG2 cells. The authors showed that HepaRG have a

metabolic activity more similar to PHH than HepG2, which has limited basal metabolic activity and poor response to CYP inducers[101]. HepaRG is a bipotent cell line that can differentiate into biliary-like cells (BLCs) and of hepatocyte-like cells (HLCs)[18]. It is a highly proliferative progenitor cell line with high functionality of CYP450 isoforms, phase II enzymes and phase III transporters upon differentiation[18]. Lübberstedt *et al.* demonstrated that HepaRG have great potential as a surrogate for PHH, since their CYP metabolic activity was comparable. However, this cell line also presented significantly higher CYP activity than in PHH for CYP2C9, CYP2C19 and CYP2D6, at later time-points and for CYP3A4 already at day 0[98]. Besides, higher albumin production and galactose/sorbitol elimination rates were also observed for HepaRG compared with PHH[98]. HepG2 cells are high proliferative cells derived from a hepatocellular carcinoma, and one of the most widely used models for *in vitro* toxicological studies, along with primary hepatocytes[89,95,101–104]. Although this cell line features many hepatic functions, the expression and activity of CYP enzymes, responsible for drug metabolism, is barely detectable in regular 2D cultures, as mentioned above[105,106]. Nonetheless, our group and others have reported HepG2 cell models in which biosynthetic function, CYP-mediated metabolism, hepatic phenotype and cell polarization, with the presence of bile-canaliculi-like structures, were successfully achieved and improved[94,107,108].

hiPSCs can be an unlimited source of HLCs with well-characterized genetic and drug metabolization profiles, being capable of accurately predict the hepatotoxicity of compounds [109]. Stem cells have the capacity to self-renew and regenerate tissue and organ systems[110]. For instance, hiPSCs can differentiate into cells that mimic the pathophysiology of the liver disease, as such, these cells constitute an important platform for disease modeling as reviewed by Corbett *et al*[111]. However, hiPSCs lines often present karyotype abnormalities and most protocols currently available do not enable the generation of fully mature hepatocytes[112–114].

Fa2N4, are non-tumorigenic immortalized hepatic cells that were proposed as a potential PHH surrogate to assess CYP induction. It was shown that these cells have a similar morphology to that of human hepatocytes and that the inducibility of various drug-metabolizing enzymes is maintained. Furthermore, Fa2N4 are easily maintained and propagated. However, studies showed that these cells present low basal enzyme activities, only detected by sensitive analytical methods, and lower expression of several hepatic uptake transporters when compared with PHH[13,81].

1.2.2.2. Culture systems

Throughout the years, 2D hepatic cultures have been losing their spotlight in the field of liver research, since they present some limitations and do not faithfully recapitulate *in vivo* liver mechanisms[115].

PHH cultured as 2D monolayers lose their polygonal structure and hepatocyte functions, such as the production of albumin and expression of CYP450 and other metabolic enzymes, within hours[116,117].

This problem led to the development of alternative culture methods, usually by providing microenvironmental clues to the hepatocytes. The sandwich model consists of culturing a cell monolayer on top of an ECM and overlaying it with another layer of ECM. Usually, the liver ECM protein component, collagen[118], or a basement membrane mimetic, such as Matrigel[93], are employed. Although it has been reported by Bell *et al.* and by Rowe *et al.* that this model maintains cells viable for up to 14 days, due to the increased cell-ECM and cell-cell contact[119], hepatocytes dedifferentiation is still an issue[120,121]. To study both acute and chronic toxicity, there was a need to develop models that could maintain functionality for longer periods of time.

Targeting better cell characteristics (viability, phenotype and function) by a better recapitulation of the physiological conditions, culture formats in which cells are in a 3D architecture have been developed[96]. The hepatic phenotype in 3D cell structures is improved on a molecular and histological level. This is due to a maximization of cell-cell contacts that induces hepatic polarization[10,107,122]. Within the 3D structure, there is the formation of nutrient and oxygen gradients that can resemble the functional zonation seen *in vivo*[18,123]. For instance, Li *et al.* determined the toxicity of 100 drugs known to cause DILI in 2D PHH monolayer cultures and 3D cultures. The 3D PHH spheroids showed higher predictivity of the toxicity of the compounds than 2D cultures of the same PHH lot; the latter failed to detect the toxicity for many of these DILI compounds[124]. Another example is the work of Vorrink *et al.* where the transcriptional and metabolic patterns of PHH cultured in 2D and 3D were compared[125]. The authors demonstrated that PHH spheroids remained metabolically stable for at least 3 weeks, as shown by the stable expression of CYP2C8, CYP2C9 and CYP3A4[125]. On the other hand, the metabolic profile of 2D PHHs was rapidly compromised, which corroborated with the increase of GSTP1 expression, an indicator of undifferentiated hepatocytes[125]. The functional activities of CYP1A2, CYP2C8, CYP2C9, CYP2D6, and CYP3A4 were, as well, highly elevated in 3D compared to 2D culture[125]. Moreover, 3D systems have been shown to improve HepG2 morphology and functionality. Gaskell *et al.* made a comparison between 2D and 3D HepG2 cultures where they demonstrated that the spheroids could better recapitulate the liver zonation and polarization[94]. The authors showed that biosynthetic function (albumin and urea production) was higher in 3D than in 2D cultures[94]. Furthermore, spheroids were more predictive in toxicological studies, presenting higher sensitivity (lower IC50 values) to the hepatotoxins tested than 2D monolayer cultures[94]. The work of Ramaiahgari *et al.* showed an increased sensitivity to compounds known to cause DILI, when HepG2 cells were cultured in 3D compared to 2D culture. This phenomenon was suggested to be related to the enhanced phase II activity of HepG2 cells when cultured as spheroids compared to monolayers[107]. Another great advantage of 3D culture systems is the possibility of performing repeated drug exposure studies, because of the extended culture time[107]. This 3D conformation can be obtained by an array of experimental methodologies, from cell aggregation in hanging drops and culture on ultra-low attachment (ULA) surfaces (based on gravity), to hollow-fiber or stirred-tank bioreactors (based on agitation), and organ-on-a-chip systems (based on microfluidics, figure 1.6), among others[1,115].

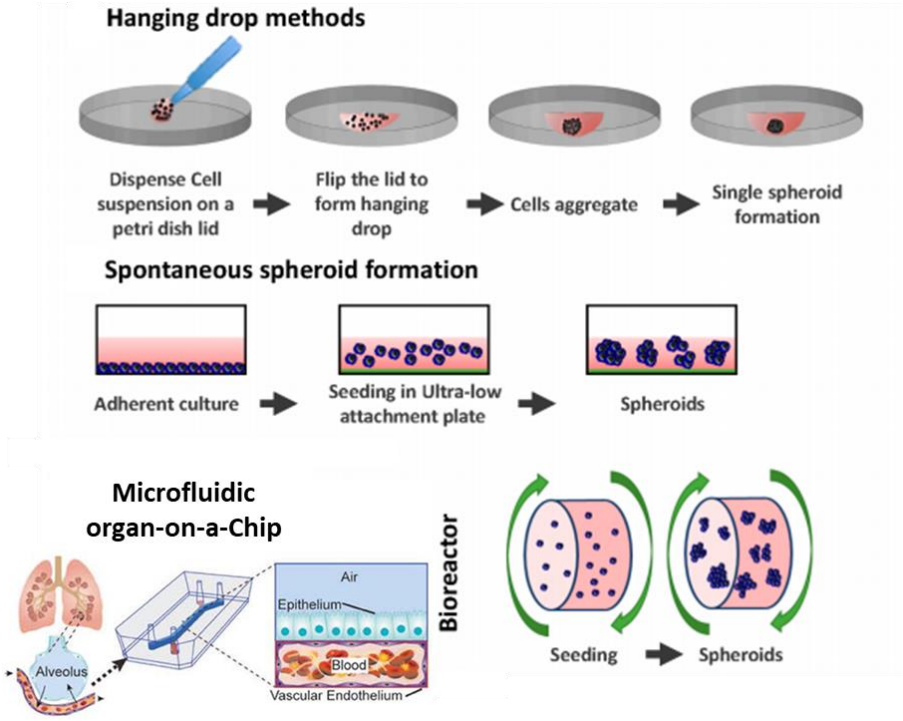

Figure 1.6. Examples of culture systems to generate spheroids. (Adapted from Hoarau-Véchot *et al.*, 2018 and Yang *et al.*, 2020)

Agitation-based systems can provide to the spheroids the necessary diffusion of soluble factors and oxygen that prevents the formation of necrotic centers[18]. Moreover, stirred-tank systems are reproducible methods, that provide long-term cultures in which spheroid morphology and size can be manipulated, adjusting the hydrodynamic conditions, and produce a high number of spheroids, making it compatible with the feeding of high-throughput screening platforms[126]. Another advantage of these systems is that it enables non-destructive sampling, ideal for continuous monitoring of culture status in the process of optimization[127].

1.2.2.3. Co-culture systems

The incorporation of different cell types to generate co-cultures increases the complexity of the model, and potentially provides a better recapitulation of the tissue and its physiology and pathophysiology, compared to monocultures[128]. Mesenchymal stem cells (MSCs) are multipotent stromal cells, capable of self-renewal and differentiation into several cell types, such as osteoblasts, adipocytes and chondroblasts. It was reported in 2D cultures that MSCs are important for supporting the proliferation, viability and improving functions of hepatocytes *in vitro*, making MSCs advantageous to use in co-culture with hepatocytes[129]. Rebelo *et al*. reported that the 3D co-culture of mesenchymal stem cells with PHH (spheroids in a stirred-tank bioreactor) improved the hepatocyte functionality[10].

Researchers aiming to study the role of the immune cells in liver inflammation and the various liver diseases have been developing co-cultures of hepatocytes, non-parenchymal cells and monocytes or macrophages from several sources. Nguyen *et al.* established a human-derived hepatocyte-KCs micropatterned co-culture (MPCC), in 96-well plates, to assess the indirect impact of cytokines in drug metabolizing enzymes and transporters[130]. The MPCC consisted of a hepatocyte pattern created by seeding these cells on rat-tail collagen type 1–patterned substrates that mediated selective cell adhesion. Murine embryonic fibroblasts were seeded 18-24h later and cryopreserved human KCs were cultured on top of this patterned layer after 7 days[130]. This model had an experimental window of approximately 2 weeks, where metabolic capacity (albumin and urea production) and functionality (CYP3A4 activity and cytokine secretion) were demonstrated. IL-1β treatment caused an immune modulatory response, resulting in the downregulation of CYP3A4, and of other metabolic enzymes' activity and gene expression. It was also observed an upregulation of C reactive protein (CRP) gene expression, and acute phase proteins – a-1-acid glycoprotein s(AAG) and serum amyloid A2 (SAA2) protein – indicative of inflammation[130]. Their results showed that the incorporation of KCs enhanced the IL-1β effects, and that co-cultures had increased sensitivity to cytokine stimulation compared with monocultures[130].

Another study, by Granitzny *et al.*, aiming to unravel the role of monocytes and macrophages in the onset of iDILI, established two 2D co-culture systems of two human cell lines, HepG2 and the monocyte-like cell line, THP-1.The latter was used directly and after differentiation into hepatocyte-like cells. The authors employed a membrane-insert system and seeded the HepG2 cells in the lower compartment and the monocytes or macrophages on the porous membrane in the insert. Monocultures and co-cultures, with and without non-toxic doses of proinflammatory factors (LPS, TNF), were exposed to different reference iDILI drugs. The results showed an enhanced hepatotoxicity in the co-cultures of HepG2 and monocytes co-exposed to Ketoconazole and LPS. Similarly, when the co-cultures of HepG2 and macrophages, exposed to LPS, were treated with Trovafloxacin or Diclofenac, enhanced hepatotoxicity was observed. Together, the results support the hypothesis that an inflammatory environment and the action of proinflammatory factors are critical for the development of iDILI[131].

Recently, Bell *et al.* published a 3D cell model based on co-cultures of cryopreserved PHH and a mixture of human NPCs. The model was challenged with LPS and TGF-β for functional characterization, and with APAP to study hepatotoxicity[132]. NPCs were characterized by the detection of CD68, indicative of KCs presence, and of α-SMA, a classical marker of activated stellate cells implying the presence of HSCs as well in the spheroids. The NPCs were analyzed as a mix and were proven to be active and have a protective effect against APAP‑induced hepatotoxicity. This was demonstrated by: i) higher PHH survival upon APAP treatment; ii) lower levels of APAP metabolite that causes glutathione depletion and generates reactive oxygen species, leading to cell necrosis; iii) consequently, less glutathione depletion was observed, which means less oxidative injury caused by APAP; iv) higher levels of (microRNA) miR-382 and miR-155, microRNAs that participate in liver regeneration and inflammation, respectively[132]. Even though this work provided a model to study the

effect of NPCs upon APAP-induced toxicity, the contribution of each NPC population cannot be individually assessed in the injury progression and the contribution of recruited circulating monocytes was not contemplated in this model, which is an important step in liver injury and still not entirely understood.

Recently, organoids have been important contributors to the study of liver disease. Organoids are 3D *in vitro* models that rely on the abilities of stem cells to differentiate into various cell types and to self-organize, forming 3D structures that recapitulate the cell types and some of the functions of the tissue [133]. An example is the work of Ouchi *et al*, which employed organoids containing hepatocyte-like cells, HSCs, cholangiocytes, and KCs, all derived from hiPSCs, to model steatohepatitis[134]. The authors showed that upon treatment with a free fatty acid, the organoids presented features observed in the livers of steatohepatitis patients, such as fibrosis and the release of inflammatory cytokines (IL-6, TNF-α)[134].

The models developed so far have contributed to great advances in this field. However, some are very complex, limiting their use in high throughput analysis, one of the most important steps for the drug industry. Furthermore, as already mentioned, there is still a need to recapitulate the KC repopulation that happens in the liver upon injury.

1.3. Thesis aim and scope

The aim of this project was to develop a 3D cell-based model to study immune-mediated drug hepatotoxicity and the liver inflammatory response, by integrating both the immune and hepatocyte components and assess their crosstalk. We reasoned that the differentiation of human peripheral monocytes into Kupffer-like cells (KLCs) could be driven by stimulating factors produced by hepatocytes in co-culture if the latter retained their original characteristics in long-term cultures. Therefore, we chose a 3D culture strategy, known to improve the hepatic cell phenotype – spheroids. The host lab had previous experience in this model system, having implemented spheroid cultures in stirred-tank culture vessels for PHH[135] and HepG2[108], employing spinner vessels and stirred-tank bioreactors of 30 mL to 300 ml. As a first approach, we chose the hepatic cell line, HepG2, to set up this model because of its higher availability and the host lab expertise.

Within this context, this thesis work had two specific objectives:

1. To implement the aggregation of hepatic cells in a downscale stirred-tank culture system, which allows the usage of primary monocytes. To accomplish this, different agitation conditions were tested in a recently-developed 30 mL spinner vessel, towards the generation of HepG2 spheroids. Cultures were monitored daily to assess the aggregation profile and cell viability.
2. To establish a 3D co-culture of hepatocytes and liver macrophages. HepG2 spheroids were co-cultured with monocytes isolated from human peripheral blood mononuclear cells (PBMCs), in 30 mL spinner vessels for 7 days. To verify if we could indeed generate a co-culture with

KLCs, the model was characterized at days 0 and 7. Surface receptors detection through flow cytometry and immunofluorescence microscopy were employed to assess the cellular phenotype of both cell populations.

2. Materials and methods

2.1. HepG2 2D culture

HepG2/C3A cells were originally obtained from ATCC (CRL-10741). The culture medium employed for maintenance of HepG2 was Dulbecco's Modified Eagle's Medium (DMEM), low glucose (1 g/L) supplemented with 10 % (v/v) fetal bovine serum (FBS) and 1 % (v/v) penicillin-streptomycin (Pen/Strep; 10,000 units/mL), all from Invitrogen, Thermo Fisher Scientific. Cells were expanded every 3 days in adherent cell culture t-flasks (Falcon). Briefly, cells were rinsed twice with phosphate-buffered saline (PBS; Thermo Fischer Scientific), incubated with 0.05 % trypsin-EDTA (Ethylenediamine tetraacetic acid; Thermo Fischer Scientific) for 5 minutes at 37ºC and the culture medium was used to inhibit trypsin enzymatic activity. The cell density and viability of the cell suspension were determined by the trypan blue exclusion assay (described in section 2.3.2). Cells were seeded at a cell density of $5x10^4$ cell/cm^2 and maintained in the incubator (Nuaire) at 37ºC, 5 % CO_2 in a humidified atmosphere.

2.2. HepG2 3D culture

2.2.1. Implementation of HepG2 aggregation in 30 mL spinners

HepG2 aggregation was previously established in our lab in 125 mL spinner vessels from Corning®[108]. Aiming to down-scale the 3D cultures, HepG2 aggregation was implemented in 30 mL spinners, kindly provided by Able Corporation. HepG2 were inoculated at a cell density of $3x10^5$ cell/mL in 30 mL of culture medium supplemented with 10 % of filtered FBS to reduce the possibility of cell clumping around fibers usually present in FBS. HepG2 cells were maintained under agitation, in spinner vessels, placed on a magnetic stirrer plate (2mag AG) in an incubator (Nuaire), at 37°C in 5 % CO_2. To optimize aggregation, three different agitation profiles were tested, as shown in table 2.1.

Table 2.1. Spinner agitation profiles.

Time	Strategy 1 (rpm)	Strategy 2 (rpm)	Strategy 3 (rpm)
Day 0	40	60	80
Day 1	50 – 65	70 – 85	90 – 105
Day 2	70	90	110
Day 3	70	90	110
Day 4	75	100	120
Day 5	85	110	120
Day 7	95	110 – 120	125
Day 8	95	120	125
Day 9	105	120	125
Day 10	105	120	125

The feeding of the HepG2 3D cultures was performed by the addition of DMEM supplemented with 5 % filtered FBS. The percentage of supplemented FBS was lower to reduce the formation of cell clumps. Two strategies were employed: (i) 50 % medium exchange every 3 days (at 3,5,8 days of culture) – optimized for the 125 mL spinner vessels; (ii) 30 % medium exchange every 2 days (at days 2,4,6) – to test if earlier nutrient supply would positively affect the spheroids viability. The aggregation profile (spheroid diameter and cell concentration) was assessed throughout culture time.

2.3. Establishment of HepG2: Monocyte co-cultures

The strategy followed for the establishment of the co-culture was to inoculate human monocytes with HepG2 spheroids. Monocytes were isolated from PBMCs and HepG2 cells were cultured in spinner vessels for 4 days, to induce spheroid formation.

2.3.1. Aggregation of HepG2 cells in 125 mL spinners

Although achieving HepG2 aggregation in 30 mL spinners, the cell viability was decreasing early along culture time. Therefore, a strategy previously implemented in the host laboratory, using 125 mL spinner vessels (Corning®), was employed for the aggregation of HepG2 cells[108] (table 2.2).

Table 2.2. Culture conditions for HepG2 aggregation in 125 ml spinner vessels.

Culture Medium	DMEM Low glucose+ 10% FBS filtered + 1% Pen/Strep
Environmental parameters	37ºC, 5% CO_2
Cell concentration	$3x10^5$ cell/mL
Volume	75 mL
Cell number	$22.5x10^6$ cells
Stirring rate	40-90 rpm

2.3.2. Monocyte isolation

Monocytes were isolated from frozen human PBMCs using the EasySep™ Human Monocyte Isolation Kit (#19359, StemCell Technologies) following the manufacturer's instructions. This isolation is achieved by a negative selection approach, where the non-monocytic cell fraction of PBMCs is bound to a mix of antibodies that are coupled to magnetic beads, separating them from the CD14+CD16- monocytes. Briefly, the cells were sequentially incubated with the kits' monocyte isolation cocktail and platelet removal cocktail, each for 5 minutes at room temperature. Afterwards, cells were incubated with the magnetic particles for another 5 minutes at room temperature. Finally, PBS supplemented with 2% (v/v) of FBS and 2mM of EDTA (Ethylenediamine tetraacetic acid) was added and the tube was placed into the "The BigEasy" EasySep™ Magnet (#18001, StemCell Technologies), for 2.5 minutes, at room temperature. The non-bound cell suspension, containing the monocytes, was poured into another tube.

The cell concentration was determined by the trypan blue exclusion method performed in a Fuchs-Rosenthal hemocytometer as described in 2.4.2.

In order to distinguish monocytes from HepG2 and assess their distribution in the co-culture, monocytes were labelled with CellTrace™ Violet (CellTrace; Invitrogen, ThermoFischer Scientific), a fluorescent dye that can be detected through several cell divisions [136]. This cell-permeant dye is cleaved by intracellular esterases generating highly fluorescent compounds that bind covalently to cellular amines. Cells were incubated with the CellTrace, diluted 1:1000 in PBS, for 20 minutes at 37ºC. After incubation, the cell suspension was washed to remove the excess of CellTrace and stored on ice until used for inoculation of the spinner. A fraction of the isolated monocytes was immediately processed for flow cytometry (day 0 analysis), as described in section 2.4.5.

2.3.3. Implementation of the HepG2: Monocyte Co-cultures

After 4 days of aggregation, the HepG2 spheroids were transferred into 30 mL spinners (ABLE Corporation) and immediately co-cultured with the CellTrace Violet-labeled monocytes. The culture conditions followed for the maintenance of the HepG2:monocyte co-cultures are represented in tables 2.3 and 2.4.

Table 2.3. Culture conditions for the co-culture of HepG2:monocytes and HepG2 monoculture controls.

Culture Medium	DMEM Low glucose+ 10% FBS filtered + 1% Pen/Strep	
Cell concentration	$5x10^5$ cell/mL	
Volume	30 mL	
Total cell number	$15x10^6$ cells	
	Co-culture	Monoculture
Cell Ratio (Hep: Mo)	2:1	-
[HepG2]	$3.33x10^5$ cell/mL	$5x10^5$ cell/mL
[Monocyte]	$1.67x10^5$ cell/mL	-
Number of vessels	2	1

Table 2.4. Agitation profile in 30 mL spinners.

Time	**Agitation rate (rpm)**
Day 0	80
Day 1	90
Day 2	100
Day 3	105
Day 4	
Day 5	115

The initial agitation rate was set at 80 rpm and changed throughout culture time based on the aggregation profile of the cells and their viability, which was assessed by fluorescence microscopy. The feeding regimen was performed by a 50 % media exchange with DMEM supplemented with 5 % filtered FBS at days 2 and 5 of culture.

2.3.4. Monocyte 2D culture

A 2D monocyte monoculture was prepared in parallel to the 3D co-culture (section 2.3) and differentiated into M1 and M2 macrophages employing prototypic inducers, to serve as a control of macrophage differentiation. After isolation, monocytes were resuspended in M1-Macrophage Generation Medium DXF (Promocell) or M2-Macrophage Generation Medium DXF (Promocell) to generate two distinct macrophage subtypes: pro-inflammatory (M1) or anti-inflammatory (M2) macrophages, respectively. Monocytes were plated at a final concentration of $1x10^6$ cells/mL, in a 6-well plate, 3 mL/well (two wells per each differentiation medium) and the plate was maintained in static conditions at 37ºC and 5 % CO_2. At day 6 of culture, 2 mL of medium was added. On day 7 of culture, the M1-macrophage wells were supplemented with IFN-γ (50 ng/mL) and LPS (10 ng/mL) and the M2-macrophages with IL-4 (20 ng/mL). On day 9 of culture, 100% of the medium was exchanged with fresh medium supplemented as in day 7. The analysis of monocyte differentiation into M1 and M2 macrophages was performed on day 10 of culture.

2.4. 3D Culture characterization

2.4.1. Cell viability assessment

Cell viability was monitored by fluorescence microscopy using a fluorescent live/dead assay. HepG2 spheroids were incubated with fluorescein diacetate (FDA) and propidium iodide (PI), both from Sigma-Aldrich – Merck, diluted 1:1000 in PBS. FDA is a cell membrane-permeant dye, which once inside viable cells is converted by esterases to a green fluorophore, fluorescein, labeling viable cells. PI is a fluorophore that can only penetrate cells that lost membrane integrity and by intercalating with DNA bases, labels dead cells with red fluorescence. Labeled spheroids were visualized in a fluorescence microscope (DMI6000, Leica).

2.4.2. Quantitative determination of cell concentration and viability

Culture samples were taken periodically to determine cell concentration and cell viability, using the trypan blue exclusion method in a Fuchs-Rosenthal hemocytometer. This blue cell membrane impermeant dye cannot penetrate viable cells, only cells that lost plasma membrane integrity. Whereas non-viable cells become dark blue, viable cells appear clear. This method allows the quantitative

determination of viable cell concentration (by assessing the number of viable cells *per* volume) and the percentage of viable cells (by determining the number of viable cells relative to the total number of cells). For this method, a single cell suspension is required. Thus, spheroid samples from day 1 of culture were directly diluted in 0.1 % (v/v) trypan blue solution (Thermo Fischer Scientific), whereas from day 3 of culture onwards (when cells are already organized in spheroids), spheroid trypsinization was performed prior to cell counting. Briefly, the aggregates were sedimented by centrifugation (up to 100x *g)*, for up to 2 min, washed with PBS, and incubated with trypsin for 5 min. Trypsin was inhibited by adding the culture medium with 10% FBS and cells were counted in a Fuchs-Rosenthal hemocytometer.

2.4.3. Determination of spheroid diameter

The determination of spheroid diameter was performed by importing fluorescence microscopy images of the live/dead assay into the open-source software Image J (version 1.52a). By adjusting the threshold that defines the spheroid boundaries, the software automatically determines the Feret's diameter for each one of the spheroids.

2.4.4. Phenotype characterization by immunofluorescence microscopy

For the optimization of HepG2 aggregation in 30 mL spinner vessels, HepG2 spheroids were collected for phenotypic characterization at days 3, 8, and 9 of culture. Spheroids were fixed in a solution of 4 % (w/v) paraformaldehyde (PFA, Fluka) with 4 % (w/v) sucrose (Merck) in PBS, for 20 min. After fixation, the cells were permeabilized and blocked with a solution of 0.2 % (w/v) Fish Skin Gelatin (FSG, Sigma-Aldrich) and 0.1 % (v/v) Triton X-100(TX-100, Merck) in PBS, for 30 min. Permeabilization allows the access to intracellular epitopes and the blocking step minimizes antibody unspecific binding. Incubation with primary antibodies (Table 2.5) diluted in 0.125 % FSG (w/v) and 0.1 % TX-100 (w/v) in PBS was performed for 2 h and incubation with secondary antibodies (Table 2.5) diluted in the same solution was performed for 1 h.

Table 2.5. List of antibodies used for immunofluorescence microscopy.

	Antibody	Host	Supplier	Dilution
Primary	*Anti-HNF4α*	Mouse	Abcam	1:200
	Anti-Albumin	Sheep	Abcam	1:1000
Secondary	*Alexa Fluor 647 anti-mouse IgG*	Donkey	Invitrogen, Thermo Fischer Scientific	1:500
	Alexa Fluor 594 anti-sheep IgG	Donkey	Invitrogen, Thermo Fischer Scientific	1:500

Additionally, spheroids were also incubated with FITC-conjugated phalloidin (A12379, Thermo Fischer Scientific) for 20 min and nuclei were counterstained with DAPI (Thermo Fischer Scientific) diluted in PBS for 5 min. All incubations were performed at room temperature and away from the light, and three washing steps with PBS were performed between each incubation period. After this process, spheroids were mounted in ProLong™ Gold Antifade Mountant (without DAPI, Thermo Fischer Scientific) and air-dried away from light, at room temperature, for 24 h.

For the co-cultures, the samples were collected at days 0 and 7 of culture and processed as described above, with the exception that the nuclei were not counterstained with DAPI. The spheroids were mounted in slides using ProLong™ Gold Antifade Mountant (without DAPI, Thermo Fischer Scientific) and coverslips. Spheroids were visualized using a point scan confocal microscope (SP5, Leica) and the generated images were analyzed with Image J software (version 1.52a).

2.4.5. Phenotype characterization by flow cytometry

To assess co-cultured monocytes differentiation along time, samples were collected at days 0 and 7 for flow cytometry analysis. Cells were recovered from the spinners and centrifuged at 100xg, for 1 minute, to sediment the spheroids. The supernatant containing mostly monocytes was further centrifuged at 400xg for 10 minutes, while the spheroids were trypsinized for 5 min, at 37 ºC. After inactivation of trypsin with culture medium containing 10% FBS, the cells recovered from the spheroids were added to the monocyte fraction and centrifuged at 400xg, for 10 min. The cells were resuspended in ice-cold PBS (-/-) until immunostaining. For the 2D macrophage differentiation controls, cells were recovered at day 10 of culture. Monolayers were incubated with 2 mM EDTA in PBS for up to 15 minutes and detached with a cell scraper. After recovery, the cells were centrifuged at 400xg for 10 minutes and then resuspended in PBS with 2% (v/v) FBS. To characterize the phenotype of monocytic cells along cultures, antibodies recognizing surface markers characteristic of each population were employed: CD14-AF488 (#557700, BD Biosciences) and CD16-APC (#360706, BioLegend) for monocytes; CD206-AF700 (#321132, Biolegend) and CD163-PE (#326506, Biolegend), for M2-macrophages; CD80-PE (#305208, Biolegend) for M1-macrophages; and MARCO-PE (#15-5447-42, Invitrogen) and VSIG4-APC (#17-5757-42, Invitrogen) for resident macrophages (KCs). The samples were incubated for 45 minutes with four different antibody mixtures and two were just incubated with buffer, to serve as negative controls, as shown in table 2.6.

Table 2.6. Labeling strategy for flow cytometry analysis.

Conditions		
M2-phenotype	M1-phenotype	KC-phenotype
$CD14_{AF488}$ $CD16_{APC}$ $CD206_{AF700}$ $CD163_{PE}$	$CD14_{AF488}$ $CD16_{APC}$ $CD80_{PE}$	$CD14_{AF488}$ $CD206_{AF700}$ $VSIG4_{APC}$ $MARCO_{PE}$
Dilution: 1:20 in PBS (final volume – 80 µL)		

After incubation, the samples were washed with PBS (400xg, 10 min) and analyzed in FACS Celesta cytometer. The results were analyzed with the FlowJo software.

3. Results and Discussion

3.1. Implementation of HepG2 3D cultures in 30 mL spinner vessels

Aggregation of the HepG2 cell line in stirred-tank culture systems was previously established in the host laboratory using 125 mL spinner vessels (Corning®)[108]. In this thesis, the aim was co-culturing this cell line with primary human monocytes, to which the access is limited. Thus, the first task of this work was to downscale 3D HepG2 cultures. For this purpose, we used 30 mL spinner vessels (ABLE Corporation). As these only recently became commercially available, not all the parameters required to describe the hydrodynamic conditions of this system are known. Therefore, an empirical approach was employed to implement the aggregation of HepG2 cells in this new system, based on our expertise on the aggregation of human hepatic cell lines and tumor cell lines in spinner vessels[18,108,137]. Single-cell suspensions of HepG2 were inoculated at a cell density of 3×10^5 cell/mL, in 30 mL of culture. Three aggregation strategies were tested, varying the initial stirring rate: (i) 40 rpm (strategy 1, S1), (ii) 60 rpm (strategy 2, S2) and (iii) 80 rpm (strategy 3, S3). The cultures were monitored every day to assess cell viability and follow the aggregation profile (spheroid diameter and cell concentration). Based on these readouts, we empirically adjusted the agitation rate throughout culture time (Fig. 3.1).

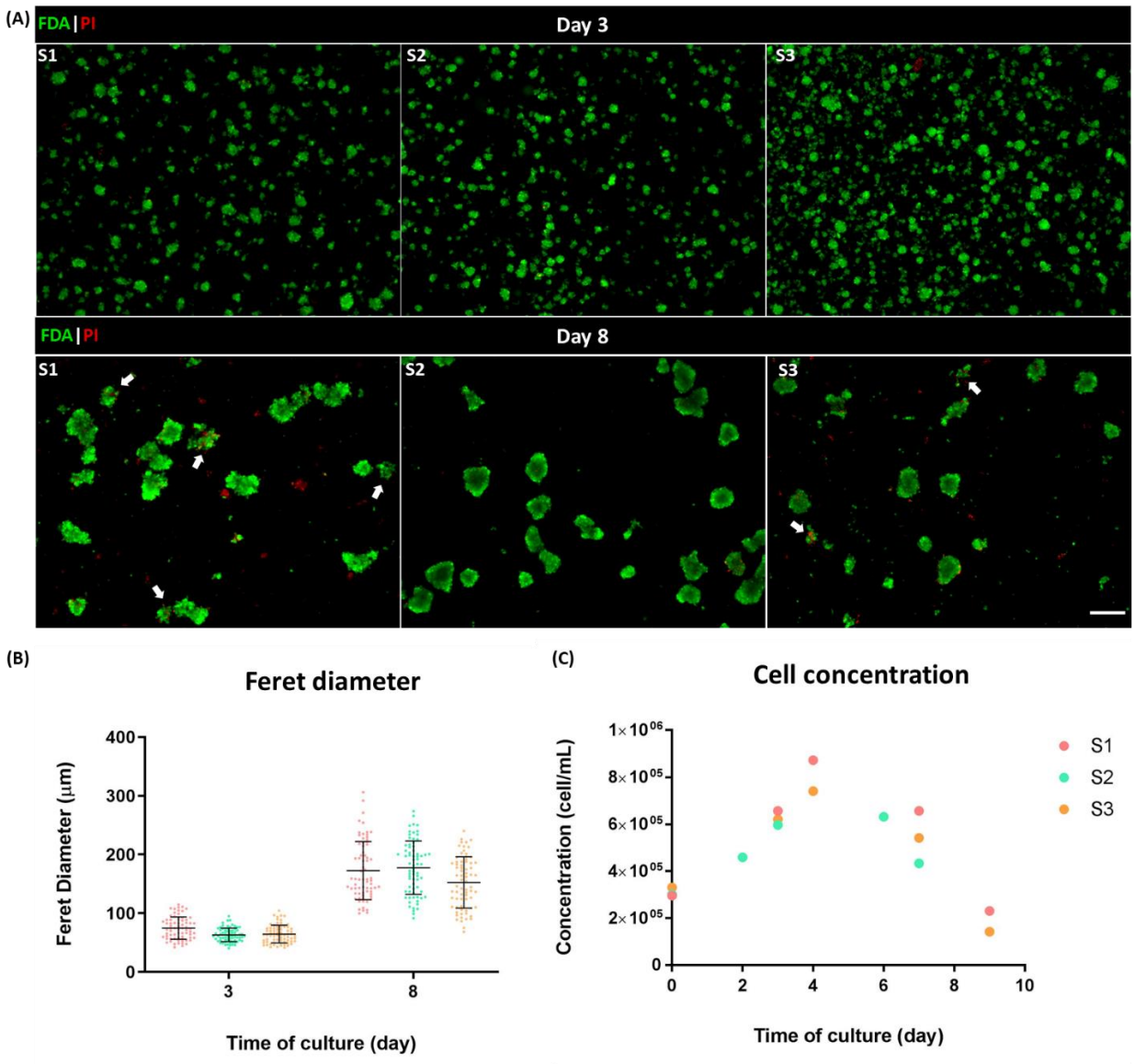

Figure 3.1 Characterization of HepG2 aggregation in 30 mL spinner vessels. (A) Representative fluorescence microscopy images of live/dead assay (Fluorescein diacetate (FDA) – green, live cells; Propidium Iodide (PI) – red, dead cells) of strategy 1 (S1), 2 (S2) and 3 (S3) at days 3 and 8 of culture. Scale bar – 250 µm. **(B)** Feret diameter of 71 spheroids from each aggregation strategy: S1, at 40 rpm; S2, at 60 rpm and S3, at 80 rpm, at days 3) and 8of culture. Mean ± S.D. **(C)** Cell concentration profile for each aggregation strategy.

By day 3 of culture, the three strategies employed generated mostly viable, compact and small aggregates with a spherical shape, termed spheroids (Fig. 3.1A). Spheroid size at day 3 of culture was similar between the three aggregation strategies, which was further corroborated by the quantitative determination of the average diameter of 71 spheroids (Fig 3.1B). These results showed that, at day 3 of culture, spheroids presented an average diameter of 74.82 µm ± 18.75, 62.25 µm ± 11.51, and 64.71 µm ± 14.96 in S1, S2 and S3, respectively. Along culture time, a tendency for increasing spheroid Feret diameter was observed; at day 8 of culture, the average was 172.61 µm ± 49.24 in S1, 177.56 µm ± 45.12 in S2 and 152.41 µm ± 43.32 in S3 (Fig. 3.1B). The higher agitation rates employed in S3 may

explain the slightly lower Ferret diameter observed in these spheroids, compared with the other strategies. Ghasemian *et al*. have shown that higher impeller speeds create higher shear stress conditions, reducing spheroid size in spinner vessels[138]. Despite the increase in spheroid size throughout culture time in all strategies, spheroids presented average diameters below 200 µm, the maximum size described without problems in the diffusion of nutrients and oxygen within spheroids[139]. It was demonstrated by Barisam *et al.* that a decrease in glucose and oxygen concentrations within spheroids, resulting from higher diameters, leads to the presence of apoptotic/necrotic centers[140]. These spheroid cores are identified by morphological features, such as cell rounding, apoptotic nuclei (pyknotic and fragmented morphology) and cell death in the center of the spheroid [141]. Indeed, we did not observe increased dead cell labeling in the central part of the spheroids (Fig. 3.1A).

At week 2 of culture, a higher heterogeneity in spheroid diameter was observed, compared to week 1 (Fig. 3.1B), which is in agreement with what was reported previously by our lab[108]. However, from week 2 onwards, loss of spheroid compactness and increased cell death were observed by the more frequent detection of propidium iodide (PI)-positive cells and lower cell packing density *per* spheroid (already visible at day 8 in S1, white arrows Fig. 3.1A)[126].

Despite the slight differences observed, the growth profiles were similar among the three aggregation strategies (Fig. 3.1C). Cells presented a proliferative profile up to day 4 of culture, after which the cell concentration started to decrease (Fig. 3.1C). The beginning of this decay corresponds to the first medium exchange, in which single cells are removed. The decrease in cell concentration was aggravated with an increase in cell death, observed in the 3D cultures at day 8 (Fig 3.1A). Furthermore, a gradual cellular attachment to the vessel and impeller was observed from day 4 onwards, leading to a considerable reduction in the spheroid number by day 10 of culture (Fig. 3.2).

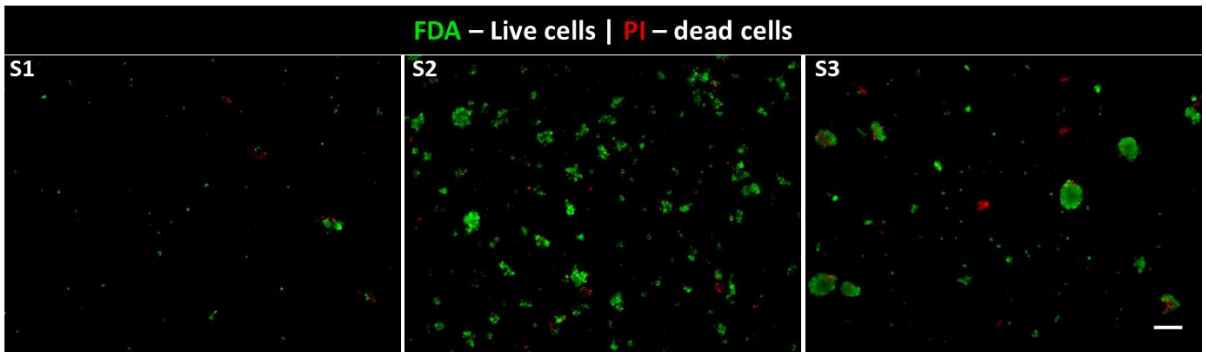

Figure 3.2. Characterization of HepG2 spheroid cultures in 30 mL spinner vessels - cell viability and spheroid morphology. Representative fluorescence microscopy images of live/dead assay. Fluorescein diacetate (FDA) – green, live cells; Propidium Iodide (PI) – red, dead cells; Strategy 1 (S1), strategy 2 (S2) and strategy 3 (S3), at week 2 of culture (day 10 for S1, S3 and day 11 for S2). Scale bar – 100 µm.

Whilst less drastically than in S1, cellular attachment to the vessel and impeller was also observed in S2 and S3. Therefore, the spheroid cultures were not maintained further than 11 days. Notably,

besides viable, spheroids generated by the three aggregation profiles also maintained hepatocyte phenotype up to week 2 of culture (Fig. 3.3).

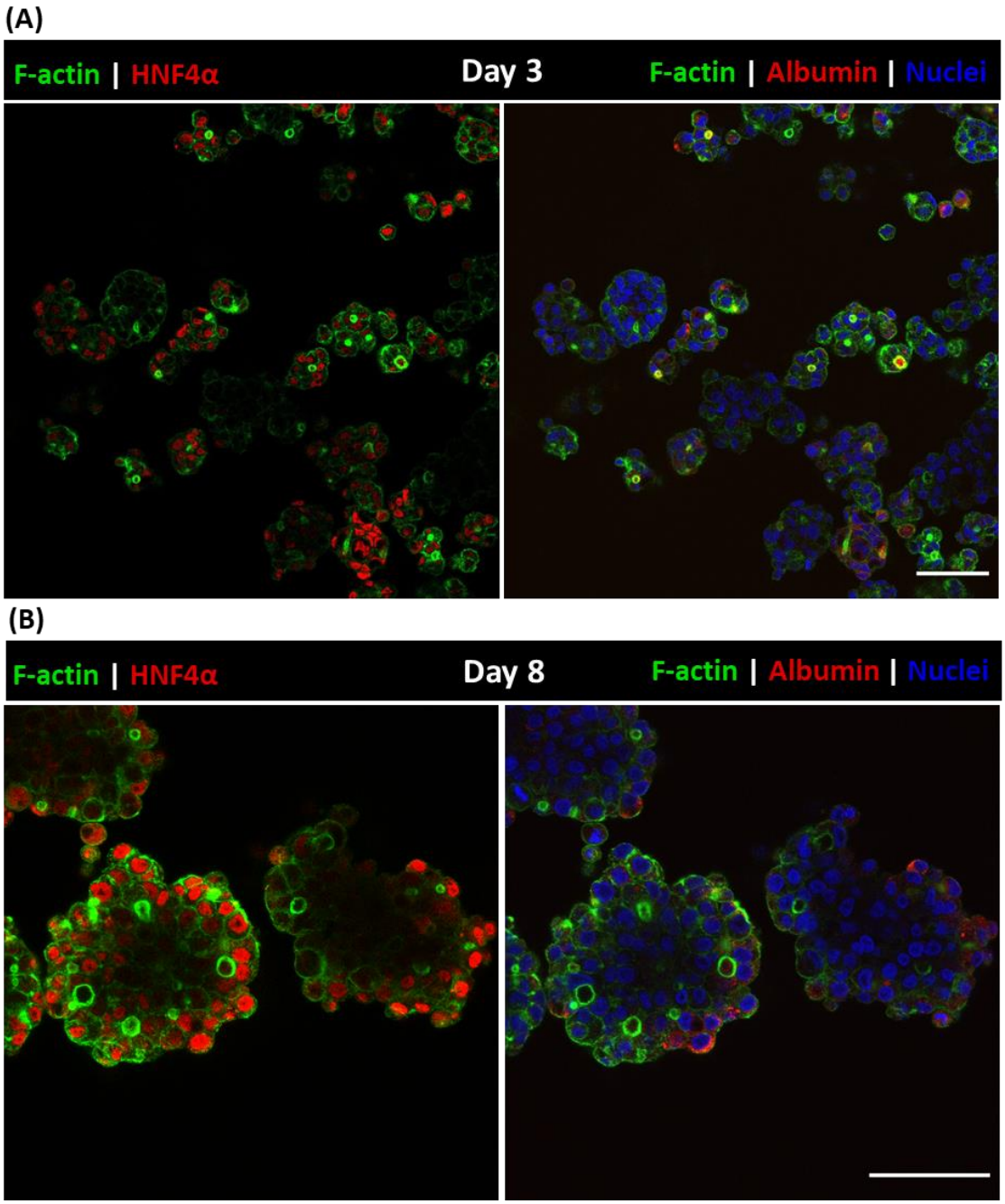

Figure 3.3. Characterization of HepG2 spheroid cultures in 30 mL spinner vessels – cell phenotype. Detection by immunofluorescence of hepatocyte nuclear factor 4 alfa (HNF4α, red) and albumin (red). F-actin was detected with phalloidin (green), and nuclei were counterstained with DAPI (blue). Images from strategy 2 at days 3 **(A)** and 8 **(B)**. Scale bars – 150 μm (up) 250 μm (down). Representative images of N=1 independent experiments.

Specifically, the cell polarization typical of hepatocytes was observed by the accumulation of F-actin filaments in the apical portion of the plasma membrane[142,143]. As our lab and others previously showed[18], the F-actin accumulation at the cellular junctions throughout the spheroid resembles the biliary-like structures, typical of polarized hepatocytes. Hepatocellular polarity is essential for liver

functions such as endocytosis, endosome distribution, glucose metabolism and signaling[142]. The hepatic identity was confirmed by the presence of the HNF4α, a nuclear transcription factor important for the liver development[51]. HNF4α is mostly expressed in mature states during hepatocyte differentiation from pluripotent stem cells[18,144], and was present in most of the cells constituting the HepG2 spheroids (Fig. 3.3). HNF4α expression is reported to be higher in 3D models than in monolayer cultures[145,146]. The biosynthetic function was assessed by the presence of albumin, a plasma protein that is synthesized by the liver[2]. Albumin was present in a fraction of the cells, as described for HepG2 cell spheroids[108]. These features were maintained from day 3 to day 8 of culture.

Despite successfully obtaining hepatic spheroids at a smaller scale, the cultures were only fully viable for about 10 days. This could have happened because of manipulation issues, when taking samples from the spinners, such as an incorrect placement of the spinner on the agitation plate; the cell concentration could be inadequate for the spinner hydrodynamic conditions since HepG2 are highly proliferative. As 10 days of culture do not represent an optimal experimental window for further introducing monocytes, another strategy was employed. Hence, HepG2 aggregation was performed in 125 mL spinner vessels from Corning®; at day 4 of culture, HepG2 spheroids were transferred into the 30 mL spinners together with a single cell suspension of monocytes, to generate co-cultures (Fig. 3.4).

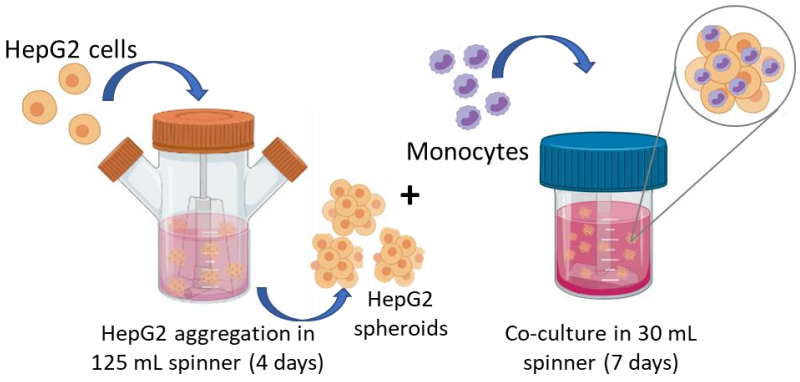

Cell density	$3x10^5$ cell/mL	$5x10^5$ cell/mL
Cell Ratio (HepG2:Monocytes)	–	2:1
Agitation speed	40 – 80 rpm	80 – 115 rpm

Figure 3.4. Experimental scheme for the HepG2 aggregation and co-culture of HepG2 cells with monocytes.

By day 4 of HepG2 aggregation in 125 mL spinners, the culture was mainly composed of compact and viable spheroids, in which HepG2 cells maintained the hepatic phenotype, as previously reported[108]. Therefore, spheroids with 4 days were selected for the co-cultures with monocytes.

In order to optimize the agitation rate in the 30 mL spinners for the culture of transferred spheroids, a 3D monoculture of HepG2 was performed. The 30 mL-spinner culture was initiated at 80 rpm, and the cell viability was assessed throughout time (Fig. 3.5).

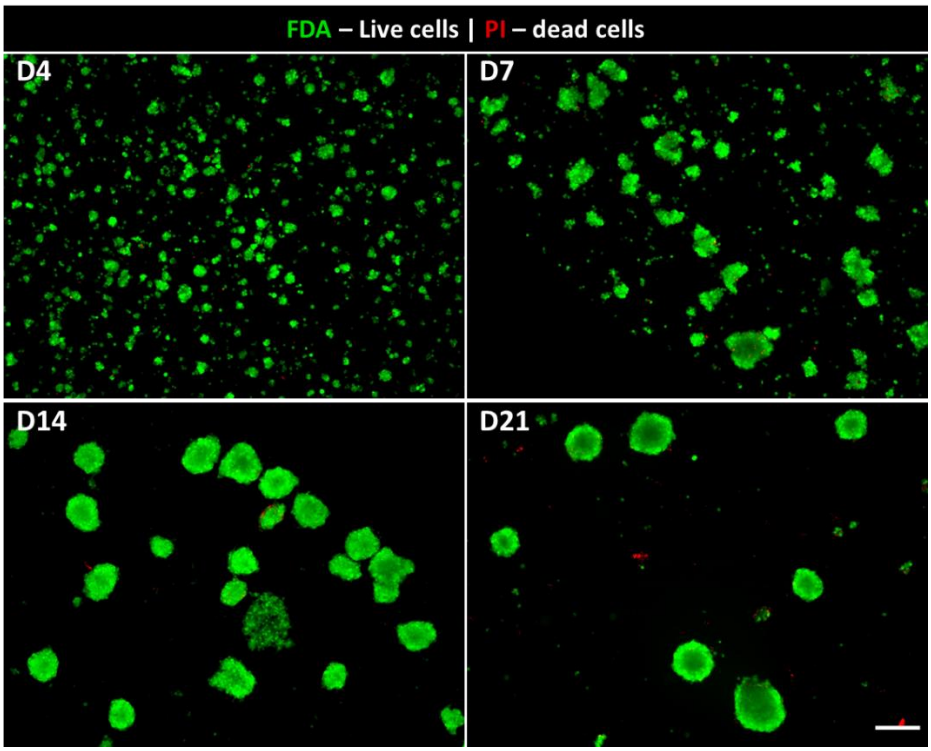

Figure 3.5. Assessment of HepG2 spheroids transferred into 30 mL spinners. Representative fluorescence microscopy images of live/dead assay (Fluorescein diacetate (FDA) – green, live cells; Propidium Iodide (PI) – red, dead cells) of spheroids at days 4, 7, 14 and 21 of culture. Scale bar – 250 μm.

Spheroids maintained high cell viability and did not fuse for as long as 17 days of culture in 30 mL spinners (Fig. 3.5). Along culture time, spheroids suffered slight changes in their morphology (e.g., at day 7 of culture) but recovered the spherical shape, without losing cell viability (Fig. 3.5). Based on cell viability and spheroid morphology, an agitation profile was established for the co-culture experiments (table 2.4, section 2).

In parallel, HepG2 spheroids maintained in the 125 mL spinner showed similar cell viability and spheroid morphology to the ones cultured in the 30 mL spinners (data not shown), suggesting that both culture formats sustained the culture of HepG2 spheroids generated in 125 mL spinners. Given the success of this approach, it was employed for the co-culture of HepG2 spheroids with human monocytes isolated from PBMCs.

3.2. Establishment of a 3D HepG2: Monocytes co-culture

As described above, monocytes were inoculated in 30 mL spinners together with HepG2 spheroids (produced in 125 mL spinners and collected at day 4, as described in section 3.1, Fig. 3.6). Based on previous studies, the ratio 2:1 (HepG2:Monocytes) was chosen for our system[132]. Three independent experiments were performed to test the hypothesis of monocyte differentiation into KLCs in culture with HepG2. To characterize the co-culture, cell viability and monocyte distribution were assessed along culture time by fluorescence microscopy (Fig. 3.6).

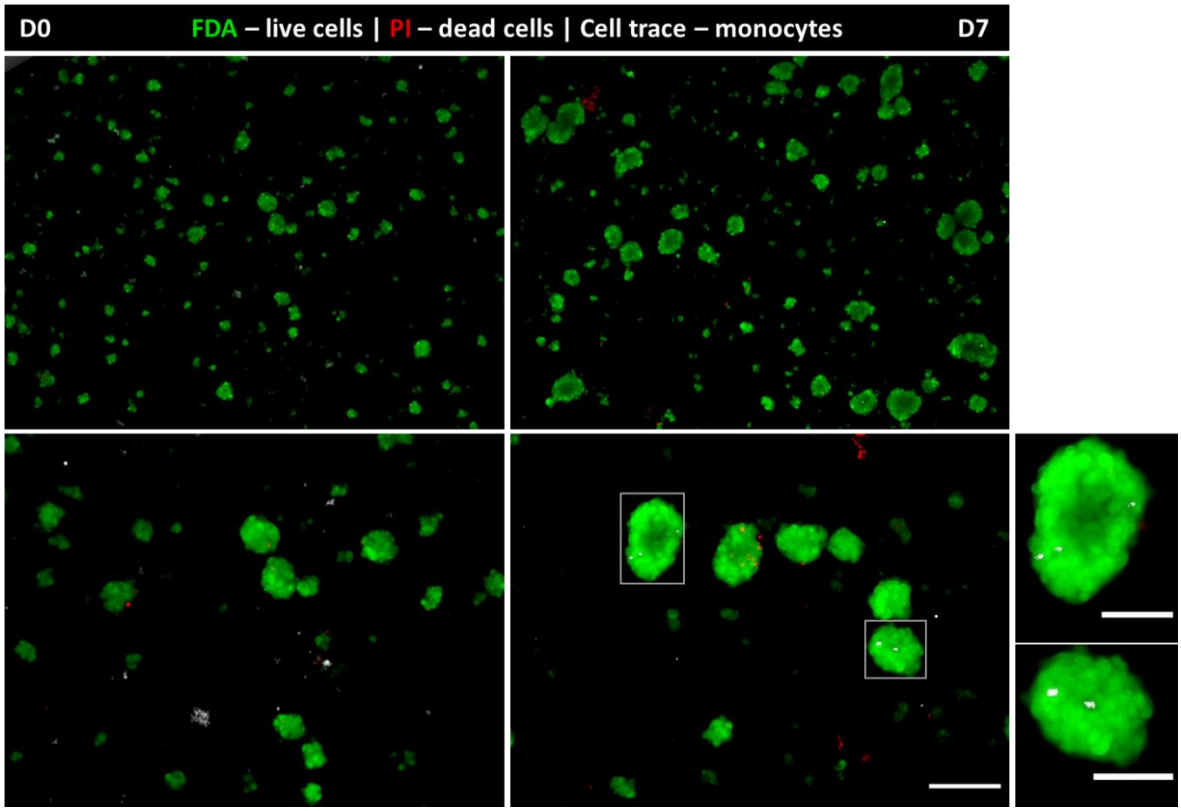

Figure 3.6. Assessment of co-cultures of HepG2 spheroids and peripheral monocytes. Representative fluorescence microscopy images of live/dead assay (Fluorescein diacetate (FDA) – green, live cells; Propidium Iodide (PI) – red, dead cells), at days 0 and 7 of co-culture. Monocytes stained with CellTrace violet – white. Scale bars – 200 μm; zoomed-in images – 100 μm.

The co-cultures were maintained for one week, along which high cell viability was observed and although showing high heterogeneity in size, the spheroids retained their compactness throughout culture time. Some of the monocytes, shown in white, were observed superimposed with the spheroids (Fig. 3.6 zoomed-in images), which suggests cell adhesion or infiltration, although this could only be verified through confocal microscopy.

As previously shown for monocultures, the HepG2 spheroids recapitulate the hepatic phenotype with the apical accumulation of F-actin filaments and the hepatic function, shown by the presence of albumin. Moreover, by labelling monocytes with the CellTrace™ dye, it was possible to observe by confocal microscopy some infiltration of immune cells into the spheroids (Fig. 3.7).

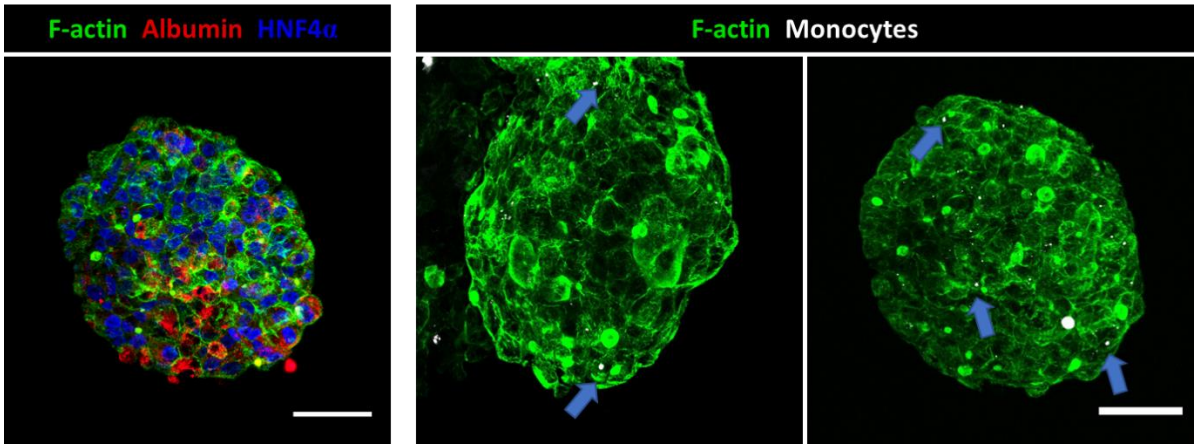

Figure 3.7.Culture characterization by immunofluorescence microscopy. Detection of F-actin (green), HNF4α (blue), albumin (red) and monocytes (white). Images from experiment 1 at day 7 of culture. Scale bars – 50 µm. Blue arrows indicate monocytes.

To characterize the phenotype of monocytes and their differentiation into macrophages along culture time, the presence of cell surface markers specific for different cell populations was evaluated by flow cytometry at days 0 and 7 of culture. The panel consisted of CD14 and CD16 for monocytes; CD80 for M1-macrophages; CD206 and CD163 for M2-macrophages and KCs; and VSIG4 and MARCO for KCs. As mentioned before, three independent experiments were performed. However, the number of cells retrieved from the first two experiments was not sufficient to perform a thorough characterization; therefore experiment 3 was accounted as N=1 for this readout.

The analysis of the results was performed on FlowJo software and consisted of applying gating strategies to the samples, defining the populations of interest. The control samples, where the gates were defined, consisted of unlabeled cells that were only incubated with PBS. This strategy enabled to discard the autofluorescence of the cells when analyzing the labelled samples. On day 0, approximately 95000 monocytes isolated from PBMCs were analyzed (Fig. 3.8).

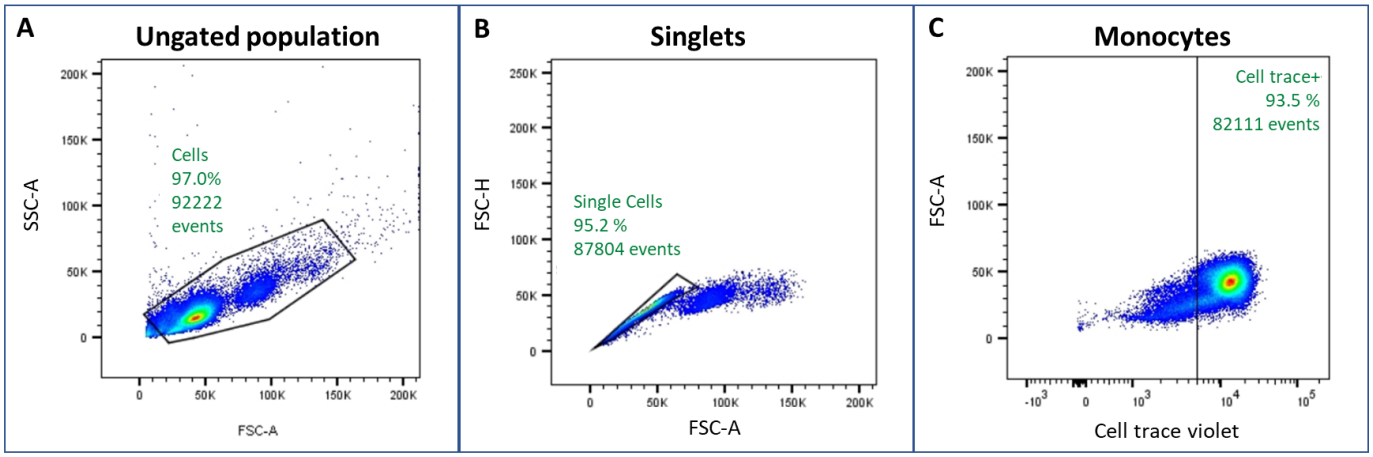

Figure 3.8 Selection of the population of interest for myeloid cell phenotype characterization by flow cytometry. Flow cytometry 2D plots of monocytes at day 0. A) Side Scatter Area (SSC-A) versus Forward Scatter Area (FSC-A), to eliminate cell debris. B) Forward Scatter Height (FSC-H) versus FSC-A to define singlets within the live cell gate. C) FSC-A versus CellTrace Violet to identify monocytes within the singlet gate.

The first gate applied (Fig. 3.8A) was to separate the live cells from the debris and dead cells based on their size (FSC-A, forward scatter area) and complexity (SSC-A, side scatter area). This resulted in a population containing 93 % of the cells assessed, 88438 events. Although the samples were filtered before analysis, some doublets pass through the strainer. To confirm the presence of doublets, cells can be plotted as illustrated in Figure 3.8B. To eliminate the doublets from the population of interest, the cells were plotted as FSC-H (forward scatter height) versus FSC-A (forward scatter area). The events that presented an enlarged area for the same height (lying outside the linear zone), indicated signal from cells that were acquired coupled to each other, and were considered the doublets[147]; the gate was applied to the single cells that appear on a diagonal. The next step was the identification of monocytes by detection of CellTrace^{+} cells in the single-cell population. The phenotype analysis was performed within this gate. The surface receptors CD14 and CD16, commonly used for monocytes characterization[50] were assessed and most of the monocytes were CD14^{+} CD16^{-} (91.6 %), characteristic of the classical blood circulating monocytes[48] (Fig. 3.9). Furthermore, this reveals a high efficiency in the isolation process since the used kit (EasySep^{TM} Human Monocyte Isolation Kit) claims to purify this specific population.

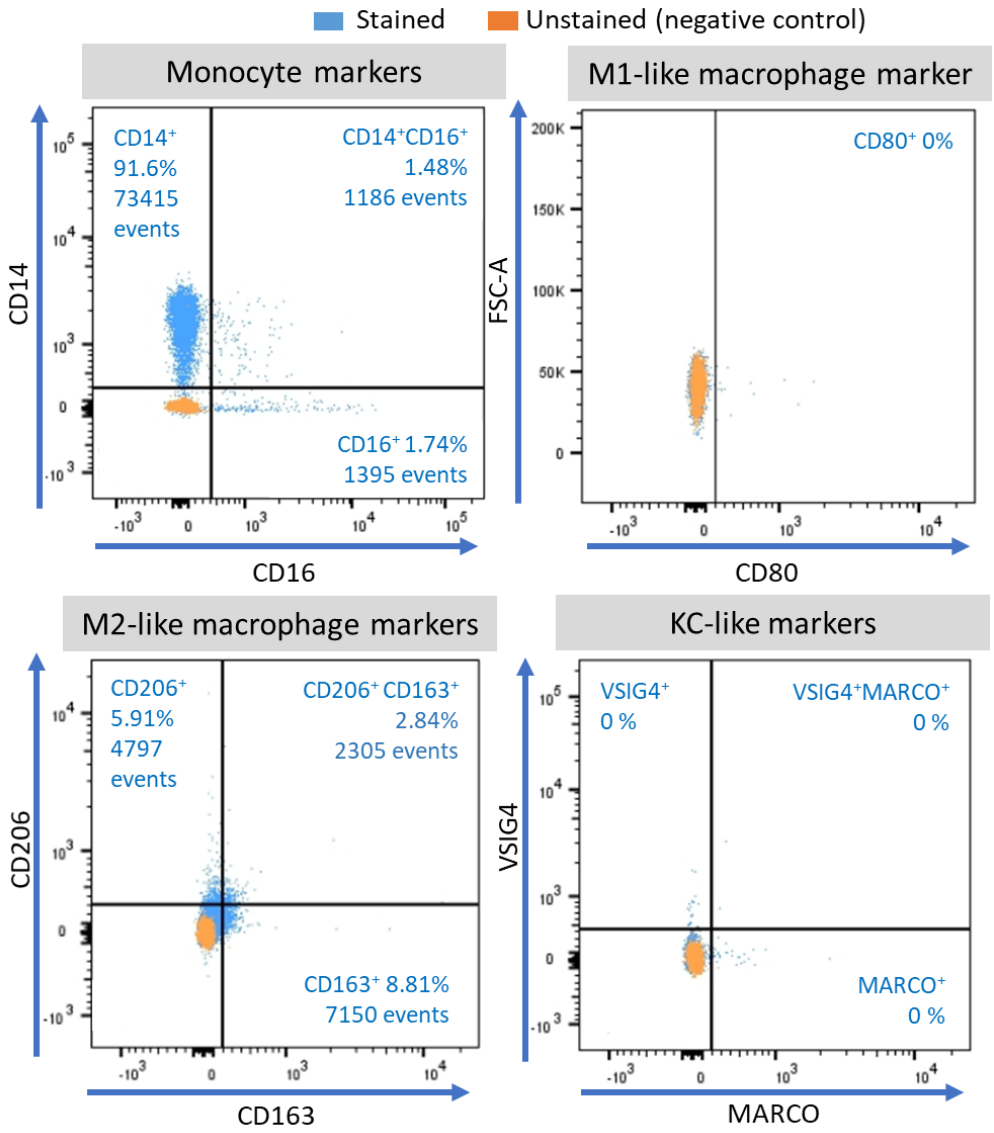

Figure 3.9. Characterization of the monocytes before co-culture (day 0). Flow cytometry 2D dot plots within the CellTrace Violet-positive population, showing the gating strategy to characterize the cell phenotype. The stained samples are represented in blue and the unstained (negative control) in orange. The percentages and number of events displayed correspond to the stained sample.

We also assessed M1-like (CD80) and M2-like (CD206, CD163) macrophage markers, to have a baseline for the differentiation analysis. CD80 was not detected in any cell, which was expected, since the sample contained peripheral blood monocytes and this marker is detected in macrophages stimulated by inflammatory stimuli[148,149]. On the other hand, few cells showed positivity for CD163 (8.81 %) and CD206 (5.91 %). There are two possible explanations for these results: i) there was unspecific antibody binding that could be excluded with an isotype control; ii) there was contamination upon the process of isolation. Since the blood was collected from apparently healthy donors, these alterations were probably not related to phenotype fluctuations that occur in sepsis and other inflammatory diseases[150,151]. Furthermore, the substantially low median fluorescence intensity (MFI) observed for CD206 and CD163

in these cells at day 0 (120 and 81.4 Arbitrary Fluorescence Units (AFU), respectively) demonstrated that this positivity for M2 markers probably has no biological significance (Fig 3.10B).

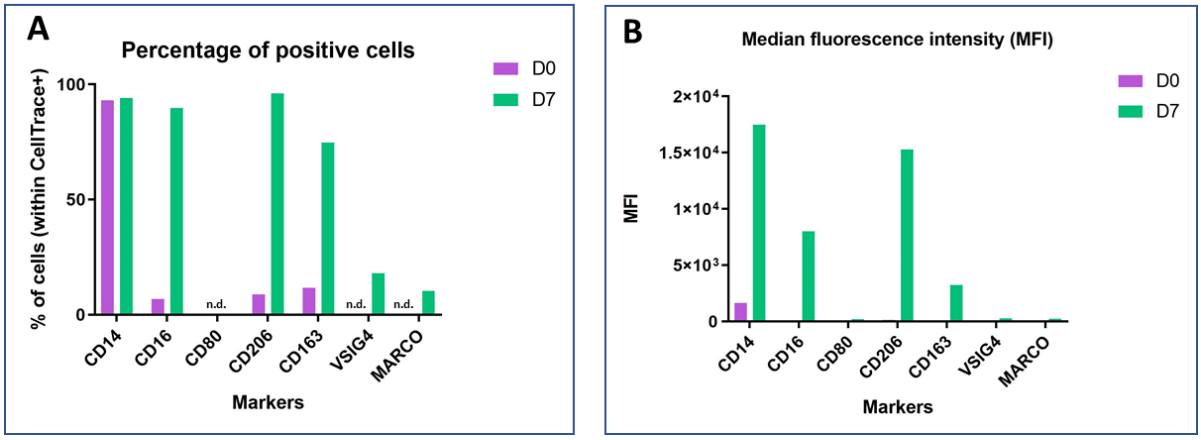

Figure 3.10. Phenotype characterization of monocytes/macrophages in co-cultures of HepG2 spheroids and peripheral monocytes. A) Percentages of positive cells detected for each marker, analyzed within the CellTrace violet^{+} population. **B)** Median fluorescence intensity (MFI) of each marker analyzed.

Moreover, the monocytes did not express any of the KC markers (Fig. 3.9), which was in accordance with the literature, as VSIG4 and MARCO are reported to be absent or at low levels in circulating monocytes, being only expressed by inflammatory monocytes[152,153]. Overall, the monocytes that were co-cultured with HepG2 cells presented the typical phenotype of classical blood circulating monocytes[48] (Fig. 3.10A).

After 7 days of co-culture, the phenotype of the immune cells was once more assessed by flow cytometry. The same gating strategy was applied to define the population of interest (CellTrace+ cells, Fig. 3.11).

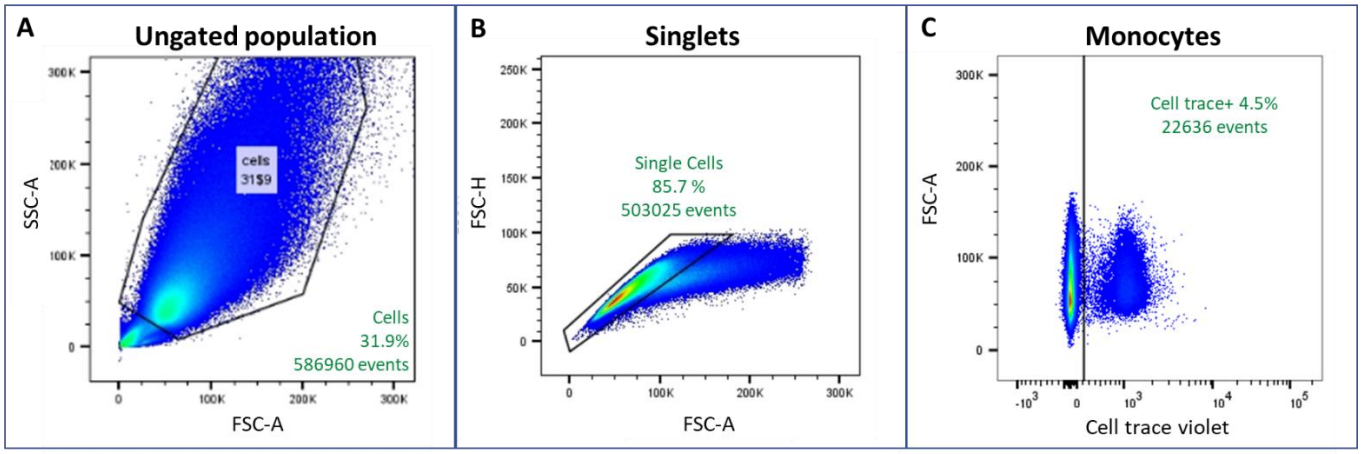

Figure 3.11. Gating strategy to define the population of interest for phenotype characterization. Flow cytometry 2D dot plots of the immune cells at day 7 of co-culture (control condition). A) Side Scatter Area (SSC-A) versus Forward Scatter Area (FSC-A) plot to eliminate cell debris. B) Forward Scatter Height versus FSC-A plot to define singlets within the live cell gate. C) FSC-A versus CellTrace Violet plot to identify monocytes within the singlet gate.

Within the co-culture, the myeloid cells accounted for 4.5 % of the total cells analyzed. The number of immune cells in the sample was expected to be low because the inoculation ratio was 2:1 (HepG2: Monocytes) and, unlike the monocytes, this hepatic cell line is highly proliferative. The decrease of $CD14^+$ cells and simultaneous increase of $CD16^+$ cells is related to activation of monocytes, suggesting that they are differentiating in the co-culture with the HepG2 cells[49] (Fig. 3.12).

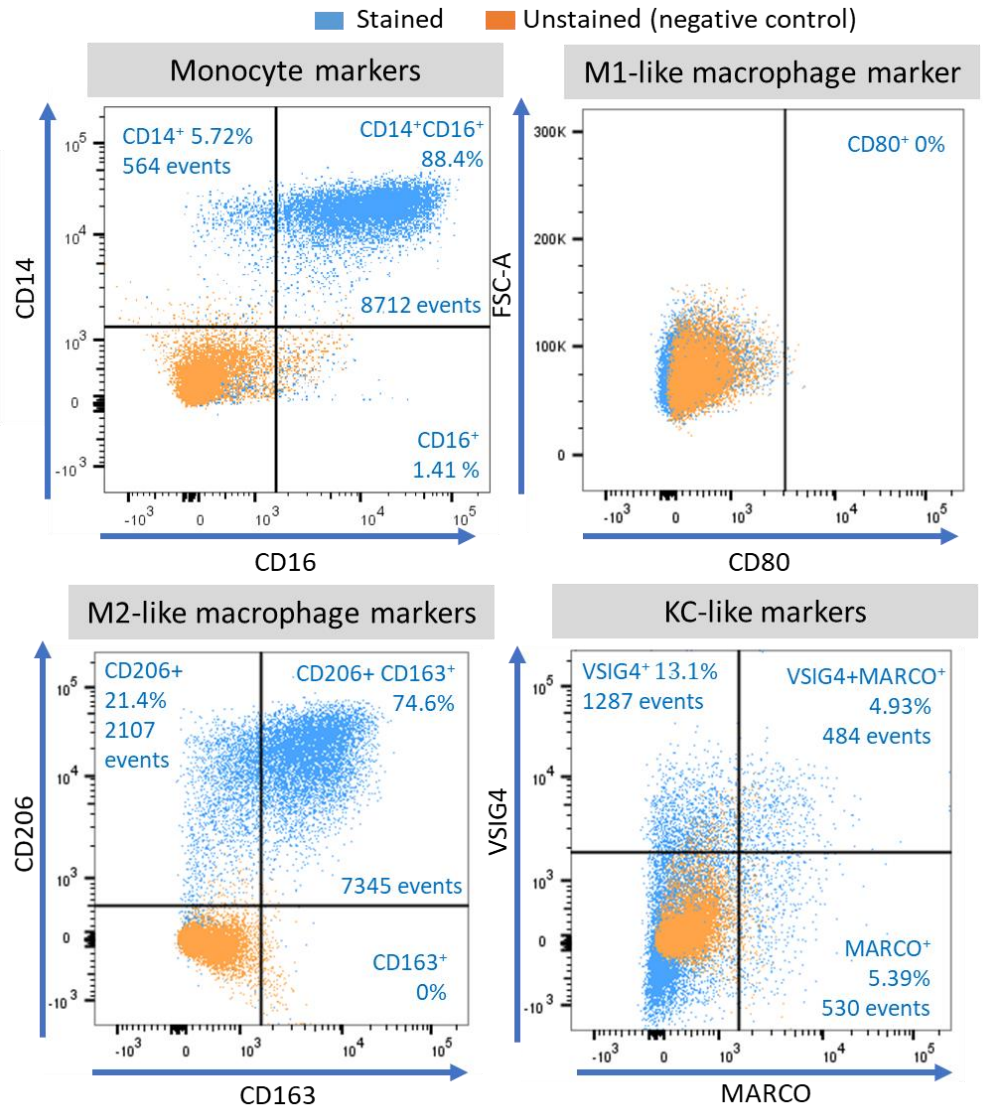

Figure 3.12. Characterization of the immune cells at day 7 of HepG2 : monocytes co-culture. Flow cytometry 2D dot plots within the CellTrace Violet-positive population, showing the gating strategy to characterize the cell phenotype. The stained samples are represented in blue and the unstained (negative control) in orange. The percentages and number of events displayed correspond to the stained sample.

When assessing M1 and M2-like macrophage markers in the sample, CD80 was not detected whilst 74.6 % of the cells were $CD206^+CD163^+$ (Fig. 3.12). Comparing with day 0, the results suggest that monocytes differentiated towards an anti-inflammatory (M2) phenotype[149]. Although a small population of cells positive for VSIG4 and MARCO was detected, the MFI for these markers was very low (Fig.3.10B). It is important to note that VSIG4 and MARCO antibodies were not validated in a positive

population before the experiment, meaning that we cannot ensure their specificity and selectivity. According to the most recent literature in human KCs, these cells are characterized by the expression of CD68, MARCO and CD163, the last two related to anti-inflammatory/tolerance responses[41]. On the other hand, monocyte-derived KCs are associated with a proinflammatory phenotype and in fact, a lower CD163 expression compared to liver-resident KCs[41,42]. These observations may suggest that in our model, the monocytes started acquiring a phenotype that is more similar to KCs in homeostasis rather than the monocyte-derived KCs phenotype. However, since we observed negligible detection of the KCs markers, we cannot take conclusions on the identity of the monocytic cells. Tumor-associated macrophages have an immunosuppressive phenotype[154], which was also described in monocytes cultured with cancer cell lines[155]. Thus, the M2-polarization of monocytes observed in our model may be due to the tumor origin of the HepG2 cells. Furthermore, the cellular crosstalk needed for the differentiation into KCs was probably not achieved, as we used a cell line that does not completely recapitulate PHH. A more complex cellular environment may be needed to achieve this, since it has been shown, in mice, that HSCs and LSECs also secrete factors that drive this differentiation[63].

In parallel, 2D monocyte cultures were performed to serve as controls for the differentiation of the monocytes. Cells were either stimulated with IFN-γ and LPS to generate M1-Mφs or with IL-4 to generate M2-Mφs. After 10 days of culture, their phenotypes were assessed as described above. Comparing the percentage of $CD14^{+}CD16^{+}$ monocytes in co-culture for 7 days with 2D controls, a similarity with the results from M2-phenotype control was observed (Figure 3.13).

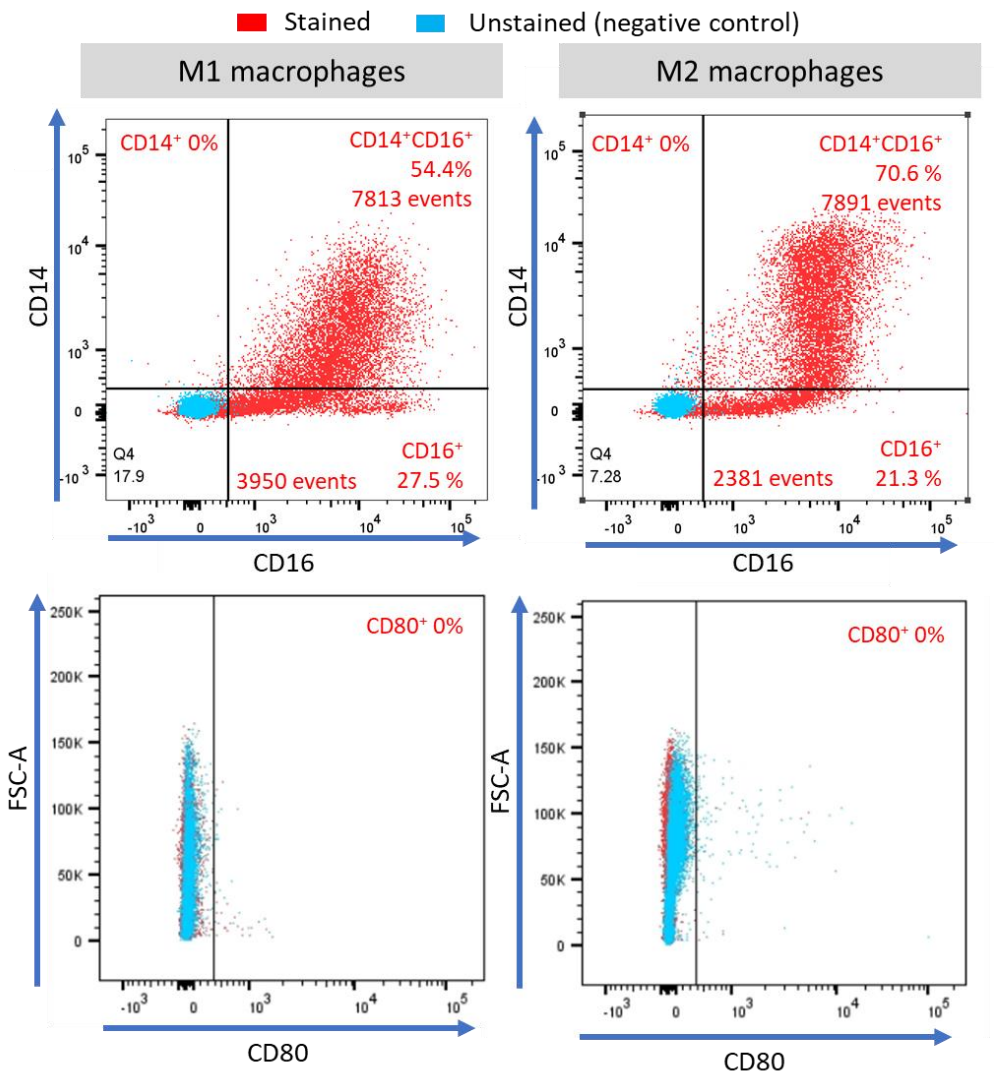

Figure 3.13. Characterization of the immune cells after 10 days of differentiation in 2D cultures. Flow cytometry 2D dot plots showing the gating strategy to characterize the cells phenotype. The stained samples are represented in red and the unstained (negative control) in blue. The percentages and number of events displayed correspond to the stained sample.

The M1-phenotype marker was not detected in any of the differentiated controls. Since this is not recurrent and even M2-Mφs usually present considerable percentages of $CD80^+$ cells (Annex 1, previous analysis from the lab) this happened because the CD80 antibody was not included in the incubation mixture. M2 markers were detected in both controls, to a less extent for M1-Mφs, as expected (Figure 3.14).

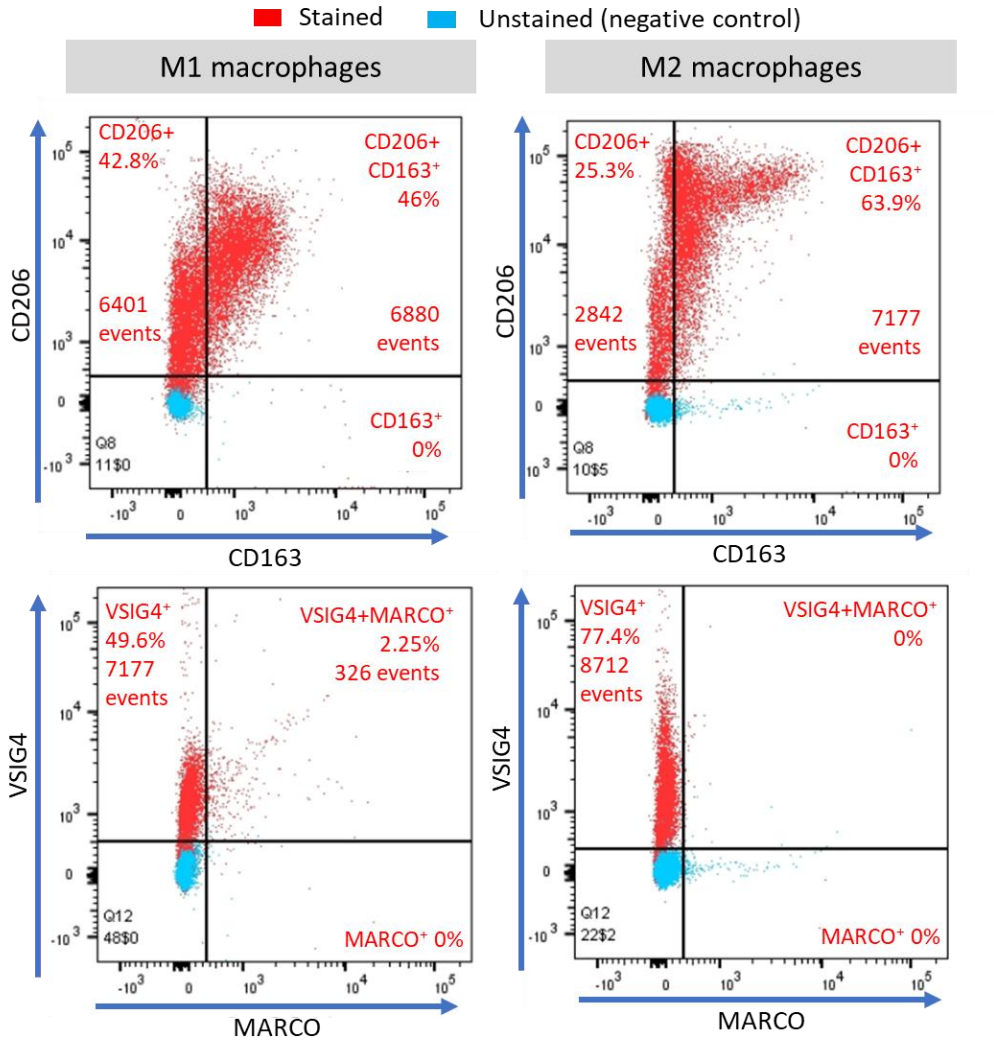

Figure 3.14. Characterization of the immune cells after 10 days of differentiation in 2D cultures. Flow cytometry 2D dot plots showing the gating strategy to characterize the cell phenotype. The stained samples are represented in *red* and the unstained (negative control) in blue. The percentages and number of events displayed correspond to the stained sample.

This was also observed in previous experiments (Annex 1), however, the previous data shows higher percentage of $CD206^{+}CD163^{+}$ cells in M2-Mφs (approximately 90%) as expected for M2-polarized Mφs. Again, the monocytes in co-culture showed a similar profile to 2D M2-Mφs rather than M1, with 74% $CD206^{+}CD163^{+}$ cells. Regarding KC markers, considerable percentages of $VSIG4^{+}$ cells were detected in both controls, contrarily to what was observed in our co-culture samples. This was observed as well in another 2D differentiation experiment (Annex 1, where the percentage of $VSIG4^{+}$ cells was higher than 80%. Overall, the controls corroborate the observations that the monocytes cultured with HepG2 differentiated into M2-like Mφs.

4. Conclusions

The aggregation of HepG2 cells was successfully downscaled to 30 mL vessels, providing viable spheroids that could recapitulate the hepatic phenotype and function for at least 8 days. The accumulation of F-actin filaments at the cellular junctions throughout the spheroids was indicative of cell polarization. The hepatic identity was confirmed by the detection of HNF4α, which is essential for the functional differentiation of hepatocytes and the formation of tight junctions. Detection of albumin, one of the plasma proteins produced by the liver, in a fraction of the cells, was indicative of biosynthetic functionality.

A co-culture of HepG2 cells and monocytes was established in the 30 mL spinner vessels and maintained for 7 days with high cell viability. Again, the typical hepatic phenotype and function were observed in the cultures by fluorescence microscopy detection of F-actin, HNF4α and albumin. Flow cytometry analysis of the monocytes demonstrated that differentiation occurred throughout culture time. The increase in $CD16^+$ cells indicated activation of the monocytes. Furthermore, the increase in $CD163^+$ and $CD206^+$ cells suggested that monocytes differentiated towards a M2-like Mφ phenotype. An anti-inflammatory phenotype is closer to what was observed for KCs rather than liver monocyte-derived Mφs. However, very few cells were positive for the KC markers, VSIG4 and MARCO, suggesting that monocytes did not acquire a KC-like phenotype. This could be related to the tumoral origin of HepG2 and their poor recapitulation of the hepatocyte-monocyte crosstalk that drives monocyte differentiation.

This work was a first step in the development of 3D cell-based models to study the role of monocyte-derived Mφs in liver inflammation and disease. The integration of monocytes in hepatic spheroids gives assess to the cellular crosstalk and the liver immune responses upon injury. Having this in mind, the next step of this work would be to assess the functionality of the immune cells in this system. Another important step is to translate this model to PHH:Monocyte co-cultures, since this cell source gives more physiological results than any cell line, as PHH could provide the necessary factors for the differentiation of monocytes into KLCs.

5. Bibliography

1. Lauschke, V. M., Hendriks, D. F. G., Bell, C. C., Andersson, T. B. & Ingelman-Sundberg, M. Novel 3D Culture Systems for Studies of Human Liver Function and Assessments of the Hepatotoxicity of Drugs and Drug Candidates. *Chem. Res. Toxicol.* (2016) doi:10.1021/acs.chemrestox.6b00150.

2. Underhill, G. H. & Khetani, S. R. Emerging trends in modeling human liver disease in vitro . *APL Bioeng.* **3**, 040902 (2019).

3. Hewitt, N. J. *et al.* Primary hepatocytes: Current understanding of the regulation of metabolic enzymes and transporter proteins, and pharmaceutical practice for the use of hepatocytes in metabolism, enzyme induction, transporter, clearance, and hepatotoxicity studies. *Drug Metab. Rev.* **39**, 159–234 (2007).

4. Gomez-Lechon, M., Donato, M., Castell, J. & Jover, R. Human Hepatocytes as a Tool for Studying Toxicity and Drug Metabolism. *Curr. Drug Metab.* **4**, 292–312 (2003).

5. Gomez-Lechon, M., Donato, M., Castell, J. & Jover, R. Human Hepatocytes in Primary Culture: The Choice to Investigate Drug Metabolism in Man. *Curr. Drug Metab.* **5**, 443–462 (2004).

6. Sivaraman, A. *et al.* A Microscale In Vitro Physiological Model of the Liver: Predictive Screens for Drug Metabolism and Enzyme Induction. *Curr. Drug Metab.* **6**, 569–591 (2005).

7. Racanelli, V. & Rehermann, B. The liver as an immunological organ. *Hepatology* **43**, (2006).

8. Brempelis, K. J. & Crispe, I. N. Infiltrating monocytes in liver injury and repair. *Clin. Transl. Immunol.* **5**, e113 (2016).

9. Seo, W. & Jeong, W. Il. Hepatic non-parenchymal cells: Master regulators of alcoholic liver disease? *World J. Gastroenterol.* **22**, 1348–1356 (2016).

10. Rebelo, S. P. *et al.* Three-dimensional co-culture of human hepatocytes and mesenchymal stem cells: improved functionality in long-term bioreactor cultures. *J. Tissue Engeering Regen. Med.* **11**, 2034–2045 (2015).

11. Kostadinova, R. *et al.* A long-term three dimensional liver co-culture system for improved prediction of clinically relevant drug-induced hepatotoxicity. *Toxicol. Appl. Pharmacol.* **268**, 1–16 (2013).

12. Khetani, S. R. & Bhatia, S. N. Microscale culture of human liver cells for drug development. *Nat. Biotechnol.* **26**, 120–126 (2008).

13. Godoy, P. *et al. Recent advances in 2D and 3D in vitro systems using primary hepatocytes, alternative hepatocyte sources and non-parenchymal liver cells and their use in investigating mechanisms of hepatotoxicity, cell signaling and ADME*. *Archives of Toxicology* vol. 87 (2013).

14. Bartlett, D. C., Hodson, J., Bhogal, R. H., Youster, J. & Newsome, P. N. Combined use of N-acetylcysteine and Liberase improves the viability and metabolic function of human hepatocytes isolated from human liver. *Cytotherapy* **16**, 800–809 (2014).

15. Si-tayeb, K., Lemaigre, F. P. & Duncan, S. A. Organogenesis and Development of the Liver. *Dev. Cell* **18**, 175–189 (2010).

16. Jungermann, K. Zonation of metabolism and gene expression in liver. *Histochem. Cell Biol.* **103**, 81–91 (1995).

17. Kang, Y. B. A., Eo, J., Mert, S., Yarmush, M. L. & Usta, O. B. Metabolic Patterning on a Chip:

Towards in vitro Liver Zonation of Primary Rat and Human Hepatocytes. *Sci. Rep.* **8**, 1–13 (2018).

18. Rebelo, S. P. *et al.* HepaRG microencapsulated spheroids in DMSO-free culture: novel culturing approaches for enhanced xenobiotic and biosynthetic metabolism. *Arch. Toxicol.* **89**, 1347–1358 (2015).

19. Iyer, K. R. & Sinz, M. W. Characterization of Phase I and Phase II hepatic drug metabolism activities in a panel of human liver preparations. *Chem. Biol. Interact.* **118**, 151–169 (1999).

20. Gómez-Lechón, M. J., Castell, J. V. & Donato, M. T. Hepatocytes-the choice to investigate drug metabolism and toxicity in man: In vitro variability as a reflection of in vivo. *Chem. Biol. Interact.* **168**, 30–50 (2007).

21. Van De Wetering, K. *et al.* Multidrug resistance proteins 2 and 3 provide alternative routes for hepatic excretion of morphine-glucuronides. *Mol. Pharmacol.* **72**, 387–394 (2007).

22. Blunt, M. C., Nicholson, J. P. & Park, G. R. Serum albumin and colloid osmotic pressure in survivors and nonsurvivors of prolonged critical illness. *Anaesthesia* **53**, 755–761 (1998).

23. Daujat-Chavanieu, M. & Kot, M. Albumin is a secret factor involved in multidirectional interactions among the serotoninergic, immune and endocrine systems that supervises the mechanism of CYP1A and CYP3A regulation in the liver. *Pharmacol. Ther.* **215**, 107616 (2020).

24. Lançon, A. *et al.* Human hepatic cell uptake of resveratrol: Involvement of both passive diffusion and carrier-mediated process. *Biochem. Biophys. Res. Commun.* **316**, 1132–1137 (2004).

25. Dunn, J. C. Y., Tompkins, R. G. & Yarmush, M. L. Hepatocytes in collagen sandwich: Evidence for transcriptional and translational regulation. *J. Cell Biol.* **116**, 1043–1053 (1992).

26. Gonzalez, F. J. Regulation of Hepatocyte Nuclear Factor 4α-mediated Transcription. *Drug Metab. Pharmacokinet.* **23**, 2–7 (2008).

27. Walesky, C. & Apte, U. Role of Hepatocyte Nuclear Factor 4α (HNF4α) in Cell Proliferation and Cancer. *Gene Expr.* **16**, 101–108 (2015).

28. Parviz, F. *et al.* Hepatocyte nuclear factor 4α controls the development of a hepatic epithelium and liver morphogenesis. *Nat. Genet.* **34**, 292–296 (2003).

29. Li, J., Ning, G. & Duncan, S. A. Mammalian hepatocyte differentiation requires the transcription factor HNF-4α. *Genes Dev.* **14**, 464–474 (2000).

30. Chiba, H. *et al.* Hepatocyte nuclear factor (HNF)-4α triggers formation of functional tight junctions and establishment of polarized epithelial morphology in F9 embryonal carcinoma cells. *Exp. Cell Res.* **286**, 288–297 (2003).

31. Treyer, A. & Müsch, A. Hepatocyte Polarity. in *Comprehensive Physiology* (John Wiley & Sons, Inc., 2013). doi:10.1002/cphy.c120009.

32. Harris, M. J., Kuwano, M., Webb, M. & Board, P. G. Identification of the Apical Membrane-targeting Signal of the Multidrug Resistance-associated Protein 2 (MRP2/cMOAT). *J. Biol. Chem.* **276**, 20876–20881 (2001).

33. Liaskou, E., Wilson, D. V. & Oo, Y. H. Innate immune cells in liver inflammation. *Mediators Inflamm.* **2012**, (2012).

34. Ikarashi, M. *et al.* Distinct development and functions of resident and recruited liver Kupffer cells/macrophages. *J. Leukoc. Biol.* **94**, 1325–1336 (2013).

35. Walbrun, P. *et al.* Characterization of rat and human Kupffer cells after cryopreservation. *Cryobiology* **54**, 164–172 (2007).

36. Holub, M. *et al.* Neutrophils Sequestered in the Liver Suppress the Proinflammatory Response of Kupffer Cells to Systemic Bacterial Infection. *J. Immunol.* **183**, 3309–3316 (2009).

37. Sitia, G. *et al.* Kupffer cells hasten resolution of liver immunopathology in mouse models of viral hepatitis. *PLoS Pathog.* **7**, (2011).

38. Svensson, G., Friman, S., Jacobsson, L. & Holmberg, S. B. Hepatocyte and Kupffer cell function after liver transplantation in the rat –in vivo evaluation with dynamic scintigraphy. *Liver* **15**, 189–195 (1995).

39. Joseph, B. *et al.* Kupffer cells participate in early clearance of syngeneic hepatocytes transplanted in the rat liver. *Gastroenterology* **123**, 1677–1685 (2002).

40. Perdiguero, E. G. *et al.* Tissue-resident macrophages originate from yolk sac-derived erythro-myeloid progenitors. *Exp. Hematol.* **43**, S64 (2015).

41. MacParland, S. A. *et al.* Single cell RNA sequencing of human liver reveals distinct intrahepatic macrophage populations. *Nat. Commun.* **9**, 1–21 (2018).

42. Scott, C. L. *et al.* Bone marrow-derived monocytes give rise to self-renewing and fully differentiated Kupffer cells. *Nat. Commun.* **7**, 1–10 (2016).

43. Arredouani, M. S. *et al.* MARCO Is the Major Binding Receptor for Unopsonized Particles and Bacteria on Human Alveolar Macrophages. *J. Immunol.* **175**, 6058–6064 (2005).

44. Chen, Y. *et al.* A regulatory role for macrophage class A scavenger receptors in TLR4-mediated LPS responses. *Eur. J. Immunol.* **40**, 1451–1460 (2010).

45. Jung, K. *et al.* Protective role of V-set and immunoglobulin domain-containing 4 expressed on kupffer cells during immune-mediated liver injury by inducing tolerance of liver T- and natural killer T-cells. *Hepatology* **56**, 1838–1848 (2012).

46. Gulubova, M. *et al.* Myeloid and Plasmacytoid Dendritic Cells and Cancer – New Insights. *Open Access Maced. J. Med. Sci.* **7**, 3324–3340 (2019).

47. Valatas, V. *et al.* Secretion of inflammatory mediators by isolated rat Kupffer cells: The effect of octreotide. *Regul. Pept.* **120**, 215–225 (2004).

48. Ziegler-Heitbrock, L. & Hofer, T. P. J. Toward a refined definition of monocyte subsets. *Front. Immunol.* **4**, 1–5 (2013).

49. Ziegler-Heitbrock, L. *et al.* Nomenclature of monocytes and dendritic cells in blood. *Blood* **116**, (2010).

50. Marimuthu, R. *et al.* Characterization of human monocyte subsets by whole blood flow cytometry analysis. *J. Vis. Exp.* **2018**, 1–10 (2018).

51. Mikołajczyk, T. P. *et al.* Interaction of human peripheral blood monocytes with apoptotic polymorphonuclear cells. *Immunology* **128**, 103–113 (2009).

52. Zimmermann, H. W. *et al.* Functional contribution of elevated circulating andhepatic non-classical CD14+CD16+ monocytes to inflammation and human liver fibrosis. *PLoS One* **5**, (2010).

53. Karlmark, K. R. *et al.* Hepatic recruitment of the inflammatory Gr1+ monocyte subset upon liver injury promotes hepatic fibrosis. *Hepatology* **50**, 261–274 (2009).

54. Gadd, V. L. *et al.* Altered peripheral blood monocyte phenotype and function in chronic liver disease: Implications for hepatic recruitment and systemic inflammation. *PLoS One* **11**, 1–20

(2016).

55. Matsusuhima Kouji, Larsen Christian G., Dubois, G. C. & Oppenheim, J. J. Purification and Characterization of a Novel Monocyte Chemotactic and Activating Factor. *J. Exp. Med.* **169**, 1485–1490 (1989).

56. Mellado, M. *et al.* The chemokine monocyte chemotactic protein 1 triggers Janus kinase 2 activation and tyrosine phosphorylation of the CCR2B receptor. *J. Immunol.* **161**, 805–13 (1998).

57. Yang, M. *et al.* Role of the JAK2/STAT3 signaling pathway in the pathogenesis of type 2 diabetes mellitus with macrovascular complications. *Oncotarget* **8**, 96958–96969 (2017).

58. Cambien, B., Pomeranz, M., Millet, M. A., Rossi, B. & Schmid-Alliana, A. Signal transduction involved in MCP-1-mediated monocytic transendothelial migration. *Blood* **97**, 359–366 (2001).

59. Miura, K., Yang, L., Rooijen, N. Van, Ohnishi, H. & Seki, E. Hepatic recruitment of macrophages promotes nonalcoholic steatohepatitis through CCR2. *Am. J. Physiol. Gastrointest. liver Physiol.* **302**, 1310–1321 (2012).

60. Heymann, F., Hammerich, L., Storch, D., Bartneck, M. & Huss, S. HHS Public Access. **55**, 898–909 (2015).

61. Serbina, N. V., Shi, C. & Pamer, E. G. Monocyte-mediated immune defense against murine listeria monocytogenes infection. *Adv. Immunol.* **113**, 119–134 (2012).

62. Blériot, C. *et al.* Liver-Resident Macrophage Necroptosis Orchestrates Type 1 Microbicidal Inflammation and Type-2-Mediated Tissue Repair during Bacterial Infection. *Immunity* **42**, 145–158 (2015).

63. Bonnardel, J. *et al.* Stellate Cells, Hepatocytes, and Endothelial Cells Imprint the Kupffer Cell Identity on Monocytes Colonizing the Liver Macrophage Niche. *Immunity* **51**, 638-654.e9 (2019).

64. Scott, C. L. *et al.* The Transcription Factor ZEB2 Is Required to Maintain the Tissue-Specific Identities of Macrophages. *Immunity* **49**, 312-325.e5 (2018).

65. Mass, E. *et al.* Specification of tissue-resident macrophages during organogenesis. *Science (80-.).* **353**, (2016).

66. Kegel, V. *et al.* Subtoxic Concentrations of Hepatotoxic Drugs Lead to Kupffer Cell Activation in a Human in Vitro Liver Model: An Approach to Study Dili. *Mediators Inflamm.* **2015**, (2015).

67. Wan, J. *et al.* M2 Kupffer cells promote M1 Kupffer cell apoptosis: A protective mechanism against alcoholic and nonalcoholic fatty liver disease. *Hepatology* **59**, 130–142 (2014).

68. Shen, K. *et al.* Depletion of activated hepatic stellate cell correlates with severe liver damage and abnormal liver regeneration in acetaminophen-induced liver injury. *Acta Biochim. Biophys. Sin. (Shanghai).* **43**, 307–315 (2011).

69. Adachi, Y., Bradford, B. U., Gao, W., Bojes, H. K. & Thurman, R. G. Inactivation of Kupffer cells prevents early alcohol-induced liver injury. *Hepatology* **20**, 453–460 (1994).

70. Sass, G., Koerber, K., Bang, R., Guehring, H. & Tiegs, G. Inducible nitric oxide synthase is critical for immune-mediated liver injury in mice. *J. Clin. Invest.* **107**, 439–447 (2001).

71. Ding, H. *et al.* Modulation of Kupffer cells on hepatic drug metabolism. *World J. Gastroenterol.* **10**, 1325–1328 (2004).

72. Wu, R. *et al.* Suppression of hepatocyte CYP1A2 expression by Kupffer cells via AhR

pathway: The central role of proinflammatory cytokines. *Int. J. Mol. Med.* **18**, 339–346 (2006).

73. Lu, R. J. *et al.* Clinical characteristics of drug-induced liver injury and related risk factors. *Exp. Ther. Med.* **12**, 2606–2616 (2016).

74. Reuben, A., Koch, D. G. & Lee, W. M. Drug-induced acute liver failure: Results of a U.S. multicenter, prospective study. *Hepatology* **52**, 2065–2076 (2010).

75. Wysowski, D. K. & Swartz, L. Adverse drug event surveillance and drug withdrawals in the United States, 1969-2002: The importance of reporting suspected reactions. *Arch. Intern. Med.* **165**, 1363–1369 (2005).

76. Lasser, K. E. *et al.* Timing of new black box warnings and withdrawals for prescription medications. *J. Am. Med. Assoc.* **287**, 2215–2220 (2002).

77. Bakke, O. M., Manocchia, M., de Abajo, F., Kaitin, K. I. & Lasagna, L. Drug safety discontinuations in the United Kingdom, the United States, and Spain from 1974 through 1993: A regulatory perspective. *Clin. Pharmacol. Ther.* **58**, 108–117 (1995).

78. Wang, X., Sun, R., Wei, H. & Tian, Z. High-mobility group box 1 (HMGB1)-toll-like receptor (TLR)4-interleukin (IL)-23-IL-17A axis in drug-induced damage-associated lethal hepatitis: Interaction of γδ T cells with macrophages. *Hepatology* **57**, 373–384 (2013).

79. Waddington, J. C., Meng, X., Naisbitt, D. J. & Park, B. K. Immune drug-induced liver disease and drugs. *Curr. Opin. Toxicol.* **10**, 46–53 (2018).

80. Consortium, M. G. S. *et al.* Initial sequencing and comparative analysis of the mouse genome. *Nature* **420**, 520–562 (2002).

81. Harding, J. D., Hoosier, G. L. Van, Jr. & Grieder, F. B. The Contribution of Laboratory Animals to Medical Progress—Past, Present, and Future. in *Handbook of Laboratory Animal Science - Essential Principles and Practices* (eds. Hau, J. & Schapiro, S. J.) 1–20 (2010). doi:10.1201/9781420040920.

82. Milani-Nejad, N. & Janssen, P. M. L. Small and large animal models in cardiac contraction research: Advantages and disadvantages. *Pharmacol. Ther.* **141**, 235–249 (2014).

83. Bardag-Gorce, F., French, B. A., Dedes, J., Li, J. & French, S. W. Gene expression patterns of the liver in response to alcohol: In vivo and in vitro models compared. *Exp. Mol. Pathol.* **80**, 241–251 (2006).

84. Olson, H. *et al.* Concordance of the toxicity of pharmaceuticals in humans and in animals. *Regul. Toxicol. Pharmacol.* **32**, 56–67 (2000).

85. Mikolajczak, S. A. *et al.* Plasmodium vivax liver stage development and hypnozoite persistence in human liver-chimeric mice. *Cell Host Microbe* **17**, 526–535 (2015).

86. Guo, J. *et al.* Humanized mice reveal an essential role for human hepatocytes in the development of the liver immune system. *Cell Death Dis.* **9**, (2018).

87. Mercer, D. F. *et al.* Hepatitis C virus replication in mice with chimeric human livers. *Nat. Med.* **7**, 927–933 (2001).

88. Tateno, C. *et al.* Near completely humanized liver in mice shows human-type metabolic responses to drugs. *Am. J. Pathol.* **165**, 901–912 (2004).

89. Guo, L. *et al.* Similarities and differences in the expression of drug-metabolizing enzymes between human hepatic cell lines and primary human hepatocytes. *Drug Metab. Dispos.* **39**, 528–538 (2011).

90. Laudanski, K. *et al.* Potential Pitfalls of the Humanized Mice in Modeling Sepsis. *Int. J.*

Inflam. **2018**, (2018).

91. Bility, M. T. *et al.* Generation of a humanized mouse model with both human immune system and liver cells to model hepatitis C virus infection and liver immunopathogenesis. *Nat. Protoc.* **7**, 1608–1617 (2012).

92. Langouët, S. *et al.* Inhibition of CYP1A2 and CYP3A4 by Oltipraz Results in Reduction of Aflatoxin Bt Metabolism in Human Hepatocytes in Primary Culture. *Cancer Res.* **55**, 5574–5579 (1995).

93. LeCluyse, E. *et al.* Expression and regulation of cytochrome P450 enzymes in primary cultures of human hepatocytes. *J. Biochem. Mol. Toxicol.* **14**, 177–188 (2000).

94. Gaskell, H. *et al.* Characterization of a functional C3A liver spheroid model. *Toxicol. Res. (Camb).* **5**, 1053–1065 (2016).

95. Mandon, M., Huet, S., Dubreil, E., Fessard, V. & Le Hégarat, L. Three-dimensional HepaRG spheroids as a liver model to study human genotoxicity in vitro with the single cell gel electrophoresis assay. *Sci. Rep.* **9**, 1–9 (2019).

96. Miranda, J. P. *et al.* Towards an Extended Functional Hepatocyte In Vitro Culture. *Tissue Eng. - Part C Methods* **15**, 157–167 (2009).

97. Wilkening, S., Stahl, F. & Bader, A. Hepg2 With Regard To Their Biotransformation Properties. *Drug Metab. Dispos.* **31**, 1035–1042 (2003).

98. Lübberstedt, M. *et al.* HepaRG human hepatic cell line utility as a surrogate for primary human hepatocytes in drug metabolism assessment in vitro. *J. Pharmacol. Toxicol. Methods* **63**, 59–68 (2011).

99. Donato, M., Tolosa, L. & Gómez-Lechón, M. *Culture and Functional Characterization of Human Hepatoma HepG2 Cells*. *Protocols in In Vitro Hepatocyte Research* vol. 1250 (2015).

100. Gerets, H. H. J. *et al.* Characterization of primary human hepatocytes, HepG2 cells, and HepaRG cells at the mRNA level and CYP activity in response to inducers and their predictivity for the detection of human hepatotoxins. *Cell Biol. Toxicol.* **28**, 69–87 (2012).

101. Berger, B. *et al.* Comparison of Liver Cell Models Using the Basel Phenotyping Cocktail. *Front. Pharmacol.* **7**, 1–12 (2016).

102. Knowles, B. B., Howe, C. C. & Aden, D. P. Human Hepatocellular Carcinoma Cell Lines Secrete the Major Plasma Proteins and Hepatitis B Surface Antigen. *Science (80-.).* **209**, 498–499 (1980).

103. Yokoyama, Y. *et al.* Comparison of drug metabolism and its related hepatotoxic effects in heparg, cryopreserved human hepatocytes, and HepG2 cell cultures. *Biol. Pharm. Bull.* **41**, 722–732 (2018).

104. Yoshitomi, S. *et al.* Establishment of the transformants expressing human cytochrome P450 subtypes in HepG2, and their applications on drug metabolism and toxicology. *Toxicol. Vitr.* **15**, 245–256 (2001).

105. Hart, S. N. *et al.* A comparison of whole genome gene expression profiles of HepaRG cells and HepG2 cells to primary human hepatocytes and human liver tissues. *Drug Metab. Dispos.* **38**, 988–994 (2010).

106. Gomez-Lechon, M., Donato, M., Lahoz, A. & Castell, J. Cell Lines: A Tool for In Vitro Drug Metabolism Studies. *Curr. Drug Metab.* **9**, 1–11 (2008).

107. Ramaiahgari, S. C. *et al.* A 3D in vitro model of differentiated HepG2 cell spheroids with improved liver-like properties for repeated dose high-throughput toxicity studies. *Arch.*

Toxicol. **88**, 1083–1095 (2014).

108. Arez, F. *et al.* Flexible 3d cell-based platforms for the discovery and profiling of novel drugs targeting plasmodium hepatic infection. *ACS Infect. Dis.* **5**, 1831–1842 (2019).

109. Szkolnicka, D. *et al.* Accurate Prediction of Drug-Induced Liver Injury Using Stem Cell-Derived Populations. *Stem Cells Transl. Med.* **3**, 141–148 (2014).

110. Zhang, Y., Bai, X. & Huang, C. Hepatic stem cells : existence and origin. *World J. Gastroenterol.* **9**, 201–204 (2003).

111. Corbett, J. L. & Duncan, S. A. iPSC-Derived Hepatocytes as a Platform for Disease Modeling and Drug Discovery. **6**, 1–12 (2019).

112. Al Tanoury Z, Piskunov A, R.-E. C. *et al.* Highly efficient generation of human hepatocyte–like cells from induced pluripotent stem cells. *Hepatology* **51**, 297–305 (2010).

113. Song, Z. *et al.* Efficient generation of hepatocyte-like cells from human induced pluripotent stem cells. *Cell Res.* **19**, 1233–1242 (2009).

114. Salomonis, N. *et al.* Integrated Genomic Analysis of Diverse Induced Pluripotent Stem Cells from the Progenitor Cell Biology Consortium. *Stem Cell Reports* **7**, 110–125 (2016).

115. Lauschke, V. M., Shafagh, R. Z., Hendriks, D. F. G. & Ingelman-Sundberg, M. 3D Primary Hepatocyte Culture Systems for Analyses of Liver Diseases, Drug Metabolism, and Toxicity: Emerging Culture Paradigms and Applications. *Biotechnol. J.* **14**, (2019).

116. Kiamehr, M. *et al.* Dedifferentiation of primary hepatocytes is accompanied with reorganization of lipid metabolism indicated by altered molecular lipid and miRNA profiles. *Int. J. Mol. Sci.* **20**, (2019).

117. Heslop, J. A. *et al.* Mechanistic evaluation of primary human hepatocyte culture using global proteomic analysis reveals a selective dedifferentiation profile. *Arch. Toxicol.* **91**, 439–452 (2017).

118. Ng, S. *et al.* Improved hepatocyte excretory function by immediate presentation of polarity cues. *Tissue Eng.* **12**, 2181–2191 (2006).

119. Moghe, P. V. *et al.* Culture matrix configuration and composition in the maintenance of hepatocyte polarity and function. *Biomaterials* **17**, 373–385 (1996).

120. Bell, C. C. *et al.* Comparison of hepatic 2D sandwich cultures and 3d spheroids for long-term toxicity applications: A multicenter study. *Toxicol. Sci.* **162**, 655–666 (2018).

121. Rowe, C. *et al.* Proteome-wide analyses of human hepatocytes during differentiation and dedifferentiation. *Hepatology* **58**, 799–809 (2013).

122. Bile, F., Using, C. & Sheets, N. Formation of Hepatocyte Spheroids with Structural Polarity. **16**, (2010).

123. Allen, J. W., Khetani, S. R. & Bhatia, S. N. In vitro zonation and toxicity in a hepatocyte bioreactor. *Toxicol. Sci.* **84**, 110–119 (2005).

124. Li, F., Cao, L., Parikh, S. & Zuo, R. Three-Dimensional Spheroids With Primary Human Liver Cells and Differential Roles of Kupffer Cells in Drug-Induced Liver Injury. *J. Pharm. Sci.* **109**, 1912–1923 (2020).

125. Vorrink, S. U., Ullah, S., Ingelman-sundberg, M. & Lauschke, V. M. Endogenous and xenobiotic metabolic stability of primary human hepatocytes in long-term 3D spheroid cultures revealed by a combination of targeted and untargeted metabolomics. *FASEB J.* **31**, 2696–2708 (2017).

126. Santo, V. E. *et al.* Adaptable stirred-tank culture strategies for large scale production of multicellular spheroid-based tumor cell models. *J. Biotechnol.* **221**, 118–129 (2016).

127. Serra, M., Brito, C., Correia, C. & Alves, P. M. Process engineering of human pluripotent stem cells for clinical application. **30**, (2012).

128. Leite, S. B. *et al.* Merging bioreactor technology with 3D hepatocyte-fibroblast culturing approaches: Improved in vitro models for toxicological applications. *Toxicol. Vitr.* **25**, 825–832 (2011).

129. Fitzpatrick, E. *et al.* Coculture With Mesenchymal Stem Cells Results in Improved Viability and Function of Human Hepatocytes. **24**, 73–83 (2015).

130. Nguyen, T. V. *et al.* Establishment of a hepatocyte-kupffer cell coculture model for assessment of proinflammatory cytokine effects on metabolizing enzymes and drug transporters. *Drug Metab. Dispos.* **43**, 774–785 (2015).

131. Granitzny, A. *et al.* Evaluation of a human in vitro hepatocyte-NPC co-culture model for the prediction of idiosyncratic drug-induced liver injury: A pilot study. *Toxicol. Reports* **4**, 89–103 (2017).

132. Bell, C. C. *et al.* Functionality of primary hepatic non-parenchymal cells in a 3D spheroid model and contribution to acetaminophen hepatotoxicity. *Arch. Toxicol.* (2020) doi:10.1007/s00204-020-02682-w.

133. Hofer, M. & Lutolf, M. P. Engineering organoids. *Nat. Rev. Mater.* **0123456789**, (2021).

134. Ouchi, R. *et al.* Modeling Steatohepatitis in Humans with Pluripotent Stem Cell-Derived Organoids. *Cell Metab.* **30**, 374-384.e6 (2019).

135. Tostões, R. M. *et al.* Human liver cell spheroids in extended perfusion bioreactor culture for repeated-dose drug testing. *Hepatology* **55**, 1227–1236 (2012).

136. Quah, B. J. C. & Parish, C. R. New and improved methods for measuring lymphocyte proliferation in vitro and in vivo using CFSE-like fluorescent dyes. *J. Immunol. Methods* **379**, 1–14 (2012).

137. Leite, S. B. *et al.* Three-dimensional HepaRG model as an attractive tool for toxicity testing. *Toxicol. Sci.* **130**, 106–116 (2012).

138. Ghasemian, M. *et al.* Hydrodynamic characterization within a spinner flask and a rotary wall vessel for stem cell culture. *Biochem. Eng. J.* **157**, 107533 (2020).

139. Wu, J., Rostami, M. R., Cadavid Olaya, D. P. & Tzanakakis, E. S. Oxygen transport and stem cell aggregation in stirred-suspension bioreactor cultures. *PLoS One* **9**, 1–12 (2014).

140. Barisam, M., Saidi, M. S., Kashaninejad, N. & Nguyen, N. T. Prediction of necrotic core and hypoxic zone of multicellular spheroids in a microbioreactor with a U-shaped barrier. *Micromachines* **9**, 1–19 (2018).

141. Ivanov, D. P. & Grabowska, A. M. In Vitro Tissue Microarrays for Quick and Efficient Spheroid Characterization. *SLAS Discov.* **23**, 211–217 (2018).

142. Zeigerer, A. *et al.* Functional properties of hepatocytes in vitro are correlated with cell polarity maintenance. *Exp. Cell Res.* **350**, 242–252 (2017).

143. Kimata, T. *et al.* Actin organization and hepatocyte differentiation are regulated by extracellular matrix via PI-4,5-bisphosphate in the rat. *Hepatology* **44**, 140–151 (2006).

144. Hanawa, M., Takayama, K., Sakurai, F., Tachibana, M. & Mizuguchi, H. Hepatocyte Nuclear Factor 4 Alpha Promotes Definitive Endoderm Differentiation from Human Induced

Pluripotent Stem Cells. *Stem Cell Rev. Reports* **13**, 542–551 (2017).

145. Talaei-khozani, T., Khodabandeh, Z., Jaberipour, M. & Hosseini, A. Comparison of hepatic nuclear factor-4 expression in two- and three- dimensional culture of Wharton's jelly-derived cells exposed to hepatogenic medium. *Rom. J. Morphol. Embryol.* **56**, 1365–1370 (2015).

146. Chang, T. T. & Hughes-Fulford, M. Molecular mechanisms underlying the enhanced functions of three-dimensional hepatocyte aggregates. *Biomaterials* **35**, 2162–2171 (2015).

147. Donnenberg, A. D. & Donnenberg, V. S. Rare-Event Analysis in Flow Cytometry. *Clin. Lab. Med.* **27**, 627–652 (2007).

148. Fleischer, J. *et al.* Differential expression and function of CD80 (B7-1) and CD86 (B7-2) on human peripheral blood monocytes. *Immunology* **89**, 592–598 (1996).

149. Raggi, F. *et al.* Regulation of human Macrophage M1-M2 Polarization Balance by hypoxia and the Triggering receptor expressed on Myeloid cells-1. *Front. Immunol.* **8**, 1–18 (2017).

150. Cornwell, W. D. *et al.* Activation and polarization of circulating monocytes in severe chronic obstructive pulmonary disease. *BMC Pulm. Med.* **18**, 1–10 (2018).

151. Brunialti, M. K. *et al.* Increased percentages of t helper cells producing il-17 and monocytes expressing markers of alternative activation in patients with sepsis. *PLoS One* **7**, 1–10 (2012).

152. Kobzik, L. & Swirski, F. K. MARCOing monocytes for elimination. *Sci. Transl. Med.* **6**, 1–6 (2014).

153. Vogt, L. *et al.* VSIG4, a B7 family-related protein, is a negative regulator of T cell activation. *J. Clin. Invest.* **116**, 2817–2826 (2006).

154. Mantovani, A. & Sica, A. Macrophages , innate immunity and cancer : balance , tolerance , and diversity. *Curr. Opin. Immunol.* **22**, 231–237.

155. Müller-Quernheim, U. C., Potthast, L., Müller-Quernheim, J. & Zissel, G. Tumor-cell co-culture induced alternative activation of macrophages is modulated by interferons in vitro. *J. Interf. Cytokine Res.* **32**, 169–177 (2012).

6. Annex

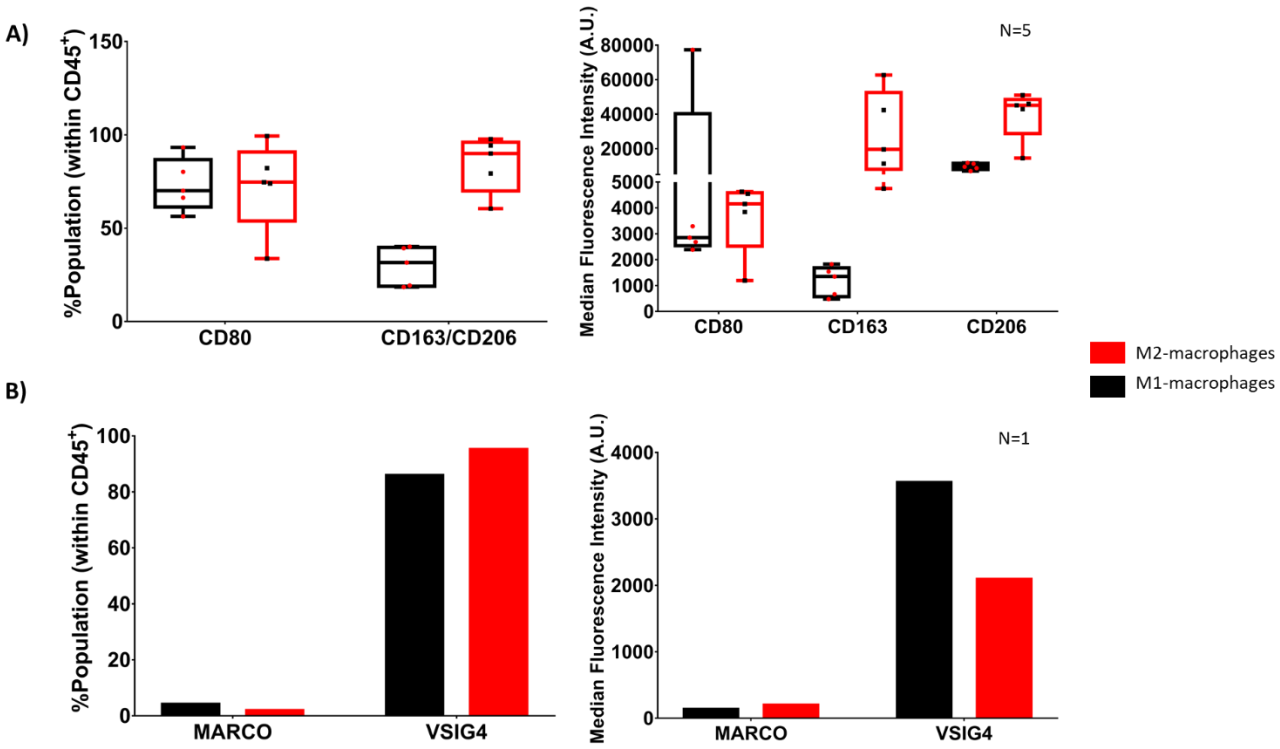

Figure 6.1. Flow cytometry data M1 and M2 macrophage phenotype. Data generated previously by the host Laboratory, on M1 and M2 macrophages differentiated in 2D, following the protocol described in the Materials and Methods. **A)** Percentages of positive cells within $CD45^+$ cells and Median Fluorescence Intensity for the markers CD80, CD163 and CD206 for M1-macrophages (black) and M2-macrophages (red). Data presented as mean ± SD of 5 independent experiments. **B)** Percentages of positive cells within $CD45^+$ cells and Median Fluorescence Intensity for the markers MARCO and VSIG4, for M1-macrophages (black) and M2-macrophages (red). Results from one independent experiment.